photonics

MDPI

Review

A Review: The Functional Materials-Assisted Terahertz Metamaterial Absorbers and Polarization Converters

Dexian Yan [1,2,3], Yi Wang [1,2,*], Yu Qiu [1], Qinyin Feng [1], Xiangjun Li [1], Jining Li [4], Guohua Qiu [1] and Jiusheng Li [1]

[1] Key Laboratory of Electromagnetic Wave Information Technology and Metrology of Zhejiang Province, College of Information Engineering, China Jiliang University, Hangzhou 310018, China; yandexian1991@163.com (D.Y.); s21030810004@cjlu.edu.cn (Y.Q.); p20030854009@cjlu.edu.cn (Q.F.); xiangjun_li@cjlu.edu.cn (X.L.); qghfr@163.com (G.Q.); lijsh2008@126.com (J.L.)
[2] State Key Laboratory of Coal Resources and Safe Mining, China University of Mining and Technology, Xuzhou 221116, China
[3] College of Information Science and Electronic Engineering, Zhejiang University, Hangzhou 310027, China
[4] College of Precision Instrument and Optoelectronic Engineering, Tianjin University, Tianjin 300072, China; jiningli@tju.edu.cn
* Correspondence: wcy16@cjlu.edu.cn

Abstract: When metamaterial structures meet functional materials, what will happen? The recent rise of the combination of metamaterial structures and functional materials opens new opportunities for dynamic manipulation of terahertz wave. The optical responses of functional materials are greatly improved based on the highly-localized structures in metamaterials, and the properties of metamaterials can in turn be manipulated in a wide dynamic range based on the external stimulation. In the topical review, we summarize the recent progress of the functional materials-based metamaterial structures for flexible control of the terahertz absorption and polarization conversion. The reviewed devices include but are not limited to terahertz metamaterial absorbers with different characteristics, polarization converters, wave plates, and so on. We review the dynamical tunable metamaterial structures based on the combination with functional materials such as graphene, vanadium dioxide (VO_2) and Dirac semimetal (DSM) under various external stimulation. The faced challenges and future prospects of the related researches will also be discussed in the end.

Keywords: metamaterial structure; functional material; absorber; polarization converter; multiple function

Citation: Yan, D.; Wang, Y.; Qiu, Y.; Feng, Q.; Li, X.; Li, J.; Qiu, G.; Li, J. A Review: The Functional Materials-Assisted Terahertz Metamaterial Absorbers and Polarization Converters. *Photonics* **2022**, *9*, 335. https://doi.org/10.3390/photonics9050335

Received: 15 April 2022
Accepted: 7 May 2022
Published: 11 May 2022

1. Introduction

The electromagnetic characteristics of optical elements, including fundamental elements and novel metamaterial structures, are determined by two factors: materials and structures [1]. For the bulk materials, the properties are based on the effects of permittivity (ε) and permeability (μ), which characterizes the polarizing capability of the material under the influence of electric and magnetic fields, respectively [2]. Metamaterials have provided novel routes for controlling electromagnetic waves and realized many excellent optical phenomena, including superlensing [3,4], electromagnetically-induced transparency [5], perfect absorption [6], polarization conversion [7], and so on. As particular subtypes, metamaterials can be treated to construct absorbers and polarization converters in terahertz frequency region, leading to near unity absorption and polarization conversion in a small or a broad frequency range. These metamaterial-based terahertz devices can be designed to break the thickness limitation of traditional quarter wavelength devices [8,9].

Dynamically manipulating electromagnetic waves based on switchable metamaterial structures can overcome the fundamental limitations of passive and static systems. In general, two main methods can be used to realize the tuning characteristics of the metamaterials. One method to achieve the tunability of the metamaterial is based on the

mechanical reconfiguration. The implementation of this method is to tune the electromagnetic responses by changing the structures, including tuning the lattice constants, resonator structures, and spatial arrangements through external stimulation. Such changes can be applied to the entire spectrum region, but generally have a long response time [10–14]. The other method is to combine the metamaterial structures with the functional materials, including liquid crystals [15], black phosphorus [16,17], graphene [1], Dirac semimetal [18], phase change materials [19], and so on, treated as surrounding media or constituent materials. This method is to modulate the optical properties of the functional materials through external stimulation, thereby further realizing the dynamic control of metamaterials. Compared to the first method, the tuning method based on functional materials can perform a faster speed with narrower operation bandwidth caused by the material dispersion [2]. This paper emphasizes recent development of functional material (including graphene, vanadium dioxide (VO_2), and Dirac semimetal (DSM))-based terahertz metamaterial structure for constructing absorbers, polarization converters and multi-functional devices in terahertz frequency band, which have no systematic summaries reported in relate review papers [1,2,6,15,20,21].

In this topical review, we demonstrate the results when terahertz metamaterial structures (mainly absorption and polarization conversion) are combined with functional materials (mainly graphene, VO_2 and DSM). We try our best to show a comprehensive insight, including the common basic structure designs and the state-of-the-art research directions. The review is organized as shown in Figure 1. Section 2 introduces the graphene-based terahertz metamaterial absorbers and polarization converters. Sections 3 and 4 summarize the VO_2- and DSM-based absorbers, polarization converters and multi-functional structures. Section 5 is focused on the realization of above functions based on the combination of two different functional materials in one metamaterial structure. Finally, conclusions and perspectives are provided in Section 6.

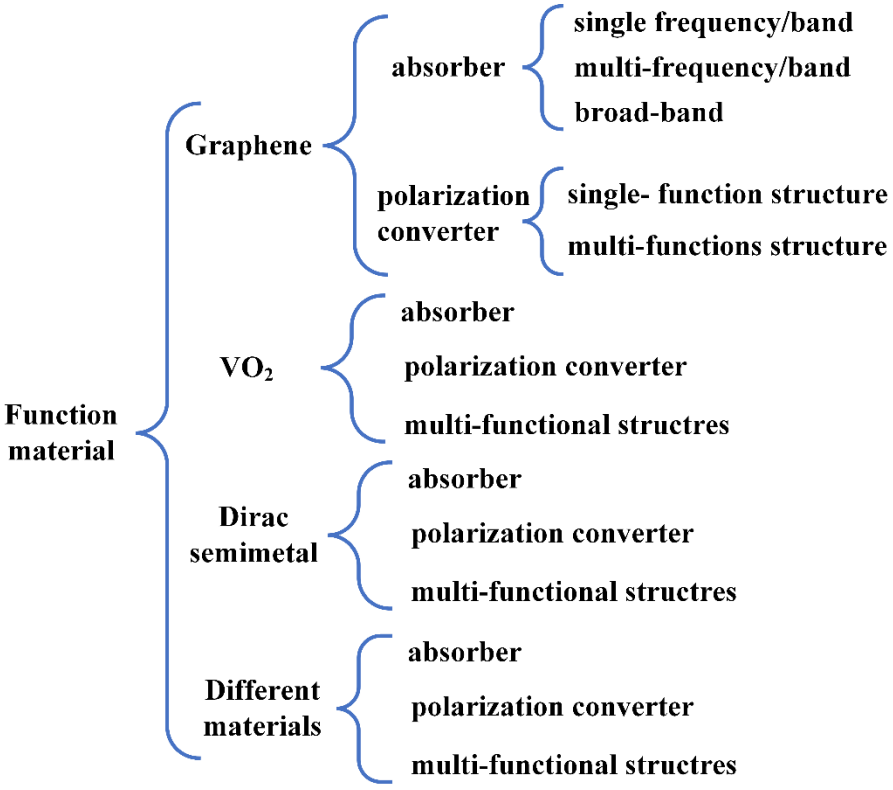

Figure 1. Organization structure of this review.

2. Graphene-Based Terahertz Metamaterial Absorbers and Polarization Converters

Graphene is a kind of two-dimensional (2D) single-layer carbon atoms exhibiting special properties [22,23]. Graphene materials can be used as an excellent platform for metamaterial and provide strong confinement. Graphene plasmons, different from the surface plasmon polarities generated by gold and copper, exhibit low loss optical properties [24]. Furthermore, the Fermi energy and the related charge carrier density can be engineered through electrical gating and doping. Higher carrier mobility (above 10,000 $cm^2/(Vs)$) has been obtained when graphene is grown by chemical vapor deposition (CVD) [25]. In addition, the mobility over 200,000 $cm^2/(Vs)$ has been achieved in the experiment by using suspended monolayer graphene [26]. Recent research demonstrates that by manufacturing the graphene layer on hexagonal Boron nitride (h-BN) substrate, the carrier mobility can reach 300,000 $cm^2/(Vs)$ at low temperature [27].

The combination of graphene and metamaterial structures allows the devices to provide better tunability. The material and structure can interact and reinforce each other; thus, the microstructures can improve the interaction of terahertz wave with the atomic thin layer of graphene, and the tunable material characteristics of graphene in turn manipulate the response of microstructures. In 2010, N. Papasimakis et al. were the first to combine the metamaterial with graphene to study the electromagnetic response of "trapped mode" plasmonic resonances [28]. They showed that the graphene dramatically changes the transmission characteristics of the designed structure, resulting in an increase in transmission of more than 250%.

In the terahertz frequency band, graphene demonstrates strong coupling effect with incident terahertz waves, and shows strong metallic characteristics when interacting with electromagnetic waves. Based on this, it allows incident waves with certain frequency to be resonantly absorbed or scattered on the graphene. Thus, the energy of electromagnetic field will be concentrated in a range of sub-wavelength range, resulting in strong graphene-based surface plasmon polaritons [29]. Since the above-mentioned advantages, graphene-based terahertz metamaterial absorbers have been extensively investigated in recent years.

2.1. Graphene-Based Terahertz Metamaterial Absorber

2.1.1. Single-Frequency/Band Terahertz Metamaterial Absorber

Treating the combination of graphene material and metamaterial structures, the tunable single-frequency/band terahertz metamaterial absorbers have been widely investigated. In general, the design methods and structures of the single-frequency/band graphene-based metamaterial absorbers are relatively simple. H. Xiong et al. reported a dynamical tunable terahertz graphene metamaterial absorber consisting of metal wire and continuous graphene film over the grounded dielectric absorber, as show in Figure 2a [30]. The frequency of the absorption peak increases from 6.91 THz to 8.1 THz, and the absorption decreases from −39.7 dB to −7.24 dB when the chemical potential increases from 0 to 0.4 eV. X. J. He et al. proposed a graphene-based metamaterial absorber to realize the active tunability of bandwidth, intensity and frequency [31]. The schematic diagram of graphene microstructure is given in Figure 2b. By varying reconfiguration state of two discs, the full width at half maximum (FWHM) bandwidth at 1.451 THz improves from 64 GHz to 96.8 GHz with no obvious resonant frequency shift, and the absorption amplitude at 1.461 THz achieves about 94% modulation depth. The resonant frequency of the absorption peak has a blueshift of 267 GHz. Furthermore, when the reconfiguration states switch between (0.09 eV and 0.12 eV) and (1.00 eV and 1.80 eV), the switching strength about 91.1% has been realized at 1.313 THz, with a corresponding switching contrast of 3961%. As illustrated in Figure 2c, Z. Yi et al. reported a switchable plasma metamaterial absorber composed of the graphene-based square-square-circle arrays [32]. Additionally, they used the structure as a refractive index sensor providing a sensitivity of 15,006 nm/RIU. Furthermore, we have designed switchable single-frequency terahertz metamaterial absorber containing a graphene microstructure layer, a silicon (Si) layer and a copper background [33]. The graphene microstructure is shown in Figure 2d, which

contains four T-shaped graphene strips and a graphene square ring. By tuning the Fermi energy of graphene based on external bias voltage, the absorption and spectral characteristics can be changed.

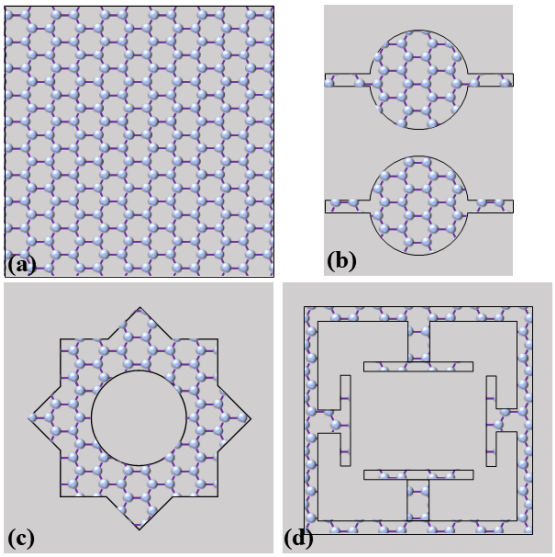

Figure 2. Graphene-based single-frequency/band terahertz metamaterial absorbers. (**a**) Metal wire and continuous graphene film; (**b**) two identical-sized graphene disc elements [31]; (**c**) square-square-circle graphene microstructure [32]; (**d**) four T-shaped graphene strips and a graphene square ring. Adapted with permission from Ref. [33], 2019, Copyright The author.

2.1.2. Dual-/Multi-Band Terahertz Metamaterial Absorbers

For the graphene-based switchable terahertz metamaterial absorbers, another research focus is to realize dual-/multi-band absorption. Two main methods can be treated to increase the absorption peaks or bands. One approach is to use the single-layer graphene microstructure to obtain the multi-band absorption. In this case, two main forms of single-layer graphene microstructures, including discrete graphene patterns and continuous microstructures, are investigated.

For discrete graphene patterns, some classical structures, including graphene elliptic structure [34–37], square patches [38,39], four T-shaped graphene strips [40–42], different sizes of graphene microstructures in one unit cell [43], graphene ribbons [44,45], perforated graphene disk [46,47], L-shaped graphene resonator [48], hexagon graphene structure [49], and so on, are used to construct the multi-band absorbers. Additionally, metamaterial absorbers based on single-layer hybrid graphene-metal structures can be used to effectively generate the multi-band absorption characteristics [50]. G. Yao et al. used the periodically patterned elliptical nanodisks graphene structure to construct a dual-band perfect absorber [34]. The cross-elliptical graphene patterns are often used in the multi-band absorbers [36,37] (as shown in Figure 3a). M. L. Huang et al. presented a dual-band terahertz metamaterial absorber using square graphene patches [39]. This absorber can realize dual-band absorption based on the excitation of fundamental and second higher-order resonant modes on square graphene patches. A dual-band perfect metamaterial absorber containing two sizes of graphene disks in one unit cell has been designed [43]. The superposition of the specific absorption peaks is caused by different disks. The resonant frequencies can be switched by changing the graphene conductivity and the geometrical parameters of the disks. J. Li et al. investigated a switchable dual-band metamaterial absorber using monolayer perforated graphene disk array with a nearly 100% absorption at 4.7 THz and 10.7 THz [46]. They used the designed structure as a refractive index sensor with the sensitivities of 0.67 THz/RIU and 2.33 THz/RIU. Y. T. Zhao et al. proposed a switchable broad-band absorber/reflector using a hybrid graphene-gold structure [50], as illustrated in Figure 3b. By changing the chemical potential (Fermi level) of the graphene from 0 to 0.3 eV,

the structure can be switched between reflector (reflection 82%) and absorber (absorption 90%) in a broad frequency band (0.53 to 1.05 THz). In Figure 3c, our group used two sizes of graphene square rings to achieve a dual-frequency tunable terahertz metamaterial absorber [51]. The absorber provides the absorption peaks of 99.8% and 99.9% at 0.74 THz and 1.71 THz. By tuning the Fermi energy of the graphene material through bias voltage, the absorption characteristics can be varied.

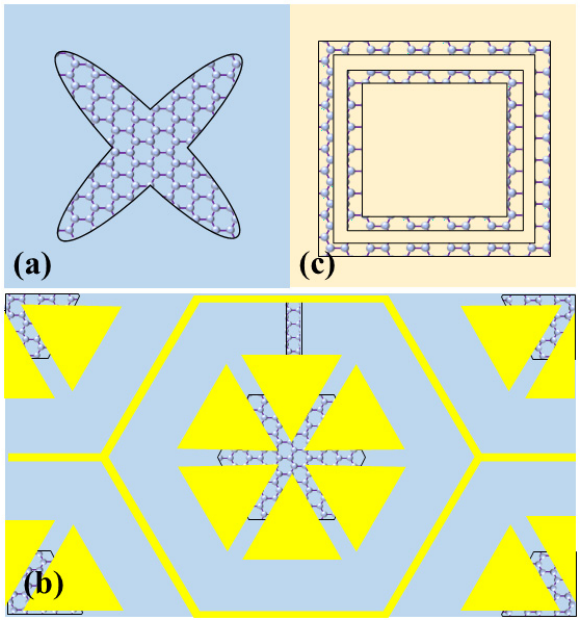

Figure 3. Graphene-based multi-band terahertz metamaterial absorbers using discrete graphene microstructures. (**a**) cross-elliptical graphene pattern [37]; (**b**) hybrid graphene-gold structure [50]; (**c**) double graphene square ring. Adapted with permission from Ref. [51], 2019, Copyright The author.

For continuous graphene microstructures, the size of graphene patterns generally needs to be consistent with the size of unit cell (periods), so that a continuous channel can be formed in the entire absorber, reducing the difficulty of processing and tuning [42,52]. Our group has conducted a lot of researches on absorbers based on continuous graphene microstructure. J. S. Li et al. presented a triple-band terahertz metamaterial absorber containing the umbrella-shaped graphene array [53]. The structure can show three absorption peaks at the frequencies of 0.506 THz, 1.638 THz, and 2.687 THz with the absorption of 0.998, 0.997 and 0.998. In Figure 4a, J. S. Li et al. reported a polarization-insensitive dual-band switchable graphene-based metamaterial absorber [54]. The graphene microstructure contains a graphene cross and graphene ring with four gaps. The frequency and intensity of the absorption peaks can be modulated based on the variation of chemical potential of graphene stimulated by external voltage. Later, in Figure 4b, we designed a switchable graphene-based metamaterial absorber using a single-layer continuous dumbbell-shaped graphene microstructure to achieve the narrow bandwidth and dual-band absorption [55]. The bandwidths of the two perfect absorption peaks are as narrow as 26.4 and 23.5 GHz with the frequencies of 224.2 GHz and 530.2 GHz, respectively.

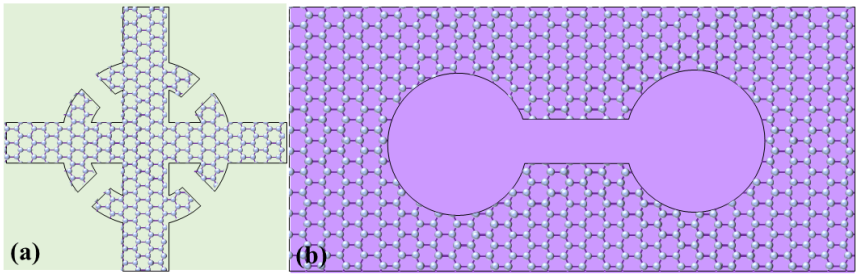

Figure 4. Graphene-based multi-band terahertz metamaterial absorbers using continuous graphene microstructures. (**a**) Graphene crossing and graphene ring with four gaps [54]; (**b**) dumbbell-shaped structure graphene [55].

For another, the patterned graphene microstructures will inevitably form truncated edges of graphene, which may result in edge effects, including unordered diffuse scattering losses [56,57]. To avoid these problems, the use of a single-layer nonstructured graphene film to form a multi-band metamaterial absorber is also a popular method [58–60]. L. M. Qi et al. used the nonstructured graphene film combined with simple dielectric resonators to obtain the broad-band and dual-band terahertz absorption [59]. The high absorption intensity of 80% can be achieved in the frequency band of 0.473–1.407 THz and 2.273–3.112 THz. Furthermore, the working function of the device can be changed between absorption (>80%) and reflection (>91%) by tuning the chemical potential of graphene. P. Jain et al. proposed a hybrid metal-graphene-based tunable polarization-insensitive metamaterial absorber to realize absorption with the properties of both broad- (absorption >90% in 4.57–6.45 THz) and dual-band absorption (6.86 TH and 7.20 THz) [60]. The normalized impedance and constitutive electromagnetic parameters of the metamaterial absorber are calculated based on the Nicolson-Ross-Weir (NRW) method to verify the absorption intensity. Two kinds of metamaterial structures with dielectric and metal resonators are given in Figure 5a,b.

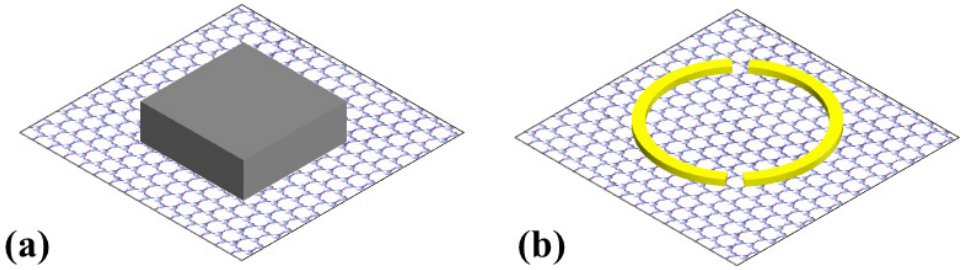

Figure 5. Graphene-based multi-band terahertz metamaterial absorbers using nonstructured graphene film. (**a**) dielectric-graphene-based structure; (**b**) Hybrid metal-graphene-based structure.

Another method to achieve multi-band absorption is stacking the multiple layers of graphene structure with different shapes and sizes [61–64]. In 2018, R. Xing et al. designed a dual-band terahertz metamaterial absorber using graphene sheet and ribbons [65]. The graphene sheet is sandwiched by SiO_2 layers and the graphene ribbons are placed on top. Based on the switchable properties of surface conductivity of graphene, the absorption can be modulated by changing the chemical potential of graphene. In 2019, Q. H. Zhou et al. designed a tunable dual-band terahertz metamaterial absorber based on cascade of a Salisbury-screen-like structure consisting of a structured graphene layer and a gold-graphene hybrid frequency selective surface (FSS) [66]. The hybrid FSS unit cell contains two gold layers separated by polyimide (PI) layer. The front gold layer is an annular aperture, and graphene material is uniformly deposited at the bottom of the annular aperture. The background layer is a gold cross structure. In 2021, P. Zamzam et al. proposed a four-band metamaterial absorber based on dual-layer graphene microstructures in the terahertz region [24]. Two layers graphene microstructures were stacked to form a four-

band metamaterial absorber providing an average absorption of 99.43% at the resonant peaks of 2.7 THz, 3.19 THz, 3.99 THz and 4.46 THz when the Fermi energy is 0.9 eV.

2.1.3. Broad-Band Terahertz Metamaterial Absorbers

In the field of broad-band applications, researchers have also adopted a variety of implementation methods. Single-layer graphene microstructure [67,68] and multi-layer graphene microstructures [69–72] have provided efficient methods for increasing the absorption bandwidth.

The first method to construct broad-band metamaterial absorbers is based on geometrical single-layer graphene microstructure. Many classical discrete graphene patterns, including target-patterned graphene resonator [73], various graphene square resonators in one unit cell [74], graphene disks [75], hexagonal spider web structure [76] and so on, are used to construct broad-band metamaterial absorbers. Furthermore, some continuous graphene layers, including continuous graphene microstructures [67,77–82] and nonstructured graphene films [68,83,84], are also used to construct the broad-band terahertz metamaterial absorbers. Y. N. Jiang et al. proposed, fabricated, and characterized a terahertz metamaterial absorber treating patterned graphene [77]. The graphene microstructure is a kind of fishnet-patterned graphene microstructures. The optimized relative bandwidths obtained from simulation and measurement are 36.6% and 14%, respectively. The resonant frequency of −1.835 THz is obtained from simulation and experiment, which satisfies the Fabry-Perot resonance condition. In 2020, J. Z. Han et al. introduced a broad-band and switchable metamaterial absorber using a sandwiched graphene microstructure [78]. As shown in Figure 6a, a single-layer graphene microstructure with hollow-out squares is treated. Plasmonic coupling and hybridization inside the graphene microstructure can greatly broaden the absorption bandwidth. The simulation results show that the absorber can provide high absorption above 90% in the frequency band of 1.14–3.31 THz with a bandwidth of 97.5%. The absorption can also be tuned from 14% to almost 100% through changing the graphene Fermi energy from 0 to 0.9 eV. In Figure 6b, R. B. Zhong et al. presented an ultra broad-band metamaterial absorber with a Si semi-ellipsoidal shape on a single-layer nonstructured graphene film that is separated by a polydimethylsiloxane layer from a bottom gold background [83]. The excellent absorption characteristics are attributed to the graphene film and the shape variation of the Si semi-ellipsoidal structure, where some discrete graphene plasmon resonances and continuous multimode Fabry-Perot resonance will be generated. The absorption bandwidth can be extended and smoothed to achieve an ultra broad-band metamaterial absorber based on the coupling of the above two resonances. The high average absorption of 95.72% can be obtained in the ultra broad-band frequency band of 2–10 THz with the relative bandwidth of 133%.

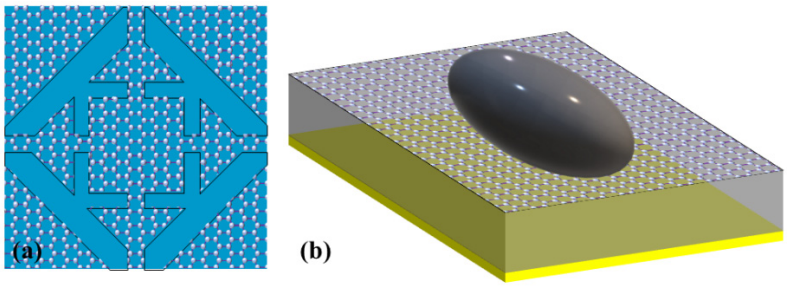

Figure 6. Graphene-based broad-band terahertz metamaterial absorbers. (**a**) structure designed by J. Z. Han et al. [78]; (**b**) a Si semi-ellipsoidal structure on a single-layer graphene film [83].

The second method to construct broad-band terahertz absorber is to use multi-layer graphene microstructures [69,70,72,85–89]. In 2018, M. Rahmanzadeh et al. proposed a polarization-insensitive metamaterial absorber on the basis of multi-layer graphene microstructures to realize an extremely broad absorption bandwidth [71]. Three graphene layers, including square, cross, and circular shapes, have been used in the absorber. The

optimized metamaterial device provides a high absorption above 90% in an ultra broad-band frequency range of 0.55–3.12 THz. In 2021, W. Liu et al. designed a kind of broad-band metamaterial perfect absorber based on the graphene and metal resonator structures [89]. The top-most pattern layer contains two concentric gold split rings and two graphene rings. The middle layer including a graphene film can be used as a Fabry-Perot cavity to improve the absorption. The bottom gold plate can be used as a reflector. High average absorption above 98.21% can be obtained in a broad-band frequency range of 4.22–7.48 THz.

Our group has designed various broad-band terahertz metamaterial absorber by treating the above methods. Wu et al. proposed a switchable and broad-band terahertz metamaterial absorber by treat a single-layer graphene-hollow-petal microstructure [90]. They used the modified Fabry-Perot resonant model to explain the mechanism. The reflection and transmission coefficients at two interfaces are calculated, and the multi-reflection process of the terahertz wave inside the dielectric layer are illustrated. A high absorption above 90% in the frequency range of 2.66–3.46 THz has been achieved. In Figure 7, J. Z. Sun et al. reported a broad-band terahertz metamaterial absorber using the asymmetric oval-shaped graphene patterns layer [91]. The absorption can be enhanced by magnetic dipole oscillations in the graphene microstructures. We have designed a broad-band graphene-based switchable metamaterial absorber composed of a graphene square ring and a combination of a graphene square ring and a solid square [92]. The optimized absorption is higher than 90% in the frequency band of 0.65–1.3 THz. Z. C. Zhai et al. proposed a broad-band metamaterial absorber based on Si strips on the continuous graphene film [93]. Based on the joint effect of Fabry-Perot resonance and the dipole mode oscillation generated by the interaction between the Si strips and graphene film, the design provides an absorption of 90% in an ultra broad-band frequency range of 0.73–1.95 THz. The operating band of the structure can be adjusted by varying the geometric parameters of Si strips and the Fermi energy of graphene.

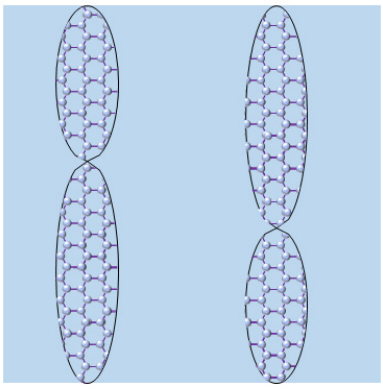

Figure 7. Broad-band terahertz metamaterial absorber based on asymmetric oval-shaped graphene patterns [91].

2.2. Graphene-Based Terahertz Metamaterial Polarization Converter

Integrating the graphene into the metamaterial structures opens a novel method to manipulate the polarization in the desired methods. In actual application, graphene-assisted metamaterial structures have indeed exhibited huge application potential in the development of high-performing terahertz polarization converters. The basic principle to design polarization converters is to use an anisotropic subwavelength microstructure made of graphene or hybrid graphene/dielectric to support two plasma intrinsic modes along two orthogonal polarization directions [1]. By changing the relative amplitude and phase delay between the two intrinsic modes based on structure design and variation of graphene conductivity, many excellent polarization conversion structures are demonstrated. The review of this part is classified by the polarization conversion with single-function and multi-function structures.

2.2.1. Graphene-Based Single-Function Metamaterial Polarization Conversion

The graphene-based metamaterial has been widely investigated for switchable polarization manipulation with single-function in terahertz region, including linear-to-cross-linear (LTL) polarization conversion (some structures: reflective sinusoidally-slotted graphene sheet [94], reflective complementary cross-shaped graphene [95], reflective nonstructured graphene film [96], and so on), linear-to-circular (LTC) polarization conversion (some structures: reflective 'I'-shaped gold structures combined with a graphene narrow strip [97], transmissive single-layer ellipse graphene patch [98], reflective I-shaped carved-hollow array [99], transmissive L-shaped graphene periodic patches [100], reflective graphene ribbon [101], reflective diamond-shaped graphene [102], and so on), circular-to-circular (CTC) polarization conversion (some structures: transmissive bi-layered complementary-oval-shaped graphene [103], transmission single-layer graphene split ring [104], and so on). In addition, some classical theories are treated to explain the mechanism of the graphene-based metamaterial polarization conversion. Y. Z. Chen et al. designed a broad-band switchable reflective polarization converter based on a single-layer complementary-cross-shaped graphene microstructure [95]. The high polarization conversion ratio (PCR) above 80% can be obtained in the frequency band of 2.15–4 THz. The physical origins are explained by field distributions and Fabry-Perot interference theory. The x-polarized component of incident terahertz wave impinging on the air-complementary-cross-shaped graphene interface is partially transmitted into the dielectric layer and partially reflected into the air. In Figure 8, R. Li et al. adopted multiple interference theory to design and investigate a graphene-assisted switchable broad-band terahertz metamaterial linear polarization converter [96]. The device provides high PCR (>0.97) and relative low ellipticity in a wide-band region of 2.68–3.93 THz. S. Quader et al. designed a broad-band LTC converter based on monolayer graphene gratings [101]. A broad-band LTC conversion with ellipticity higher than 0.95 can be obtained in the frequency range of 14–40 THz with the efficiency higher than 90%. They have derived the equivalent circuit model to explain the physical mechanism of the processes and results. For the x- and y-polarization, the cross-polarized reflection coefficients are negligible, thus the equivalent circuit model of the LTC polarization conversion structure can be separated for x and y directions. For x- and y-polarizations, the designed metamaterial structure can be modelled as a series RLC circuit and a series RL circuit, respectively. Y. Z. Cheng et al. designed a transmissive graphene-based switchable terahertz metamaterial CTC polarization converter consisted of metal gratings sandwiched with two layers of complementary-oval-shaped graphene microstructures [103]. Since the combined effect of anisotropic and Fabry–Perot-like resonance cavity enhanced effects, the converter can transform the incident right-handed circularly polarized terahertz wave to left-handed circularly polarized wave with high PCR of 99.9% at 1.1 THz.

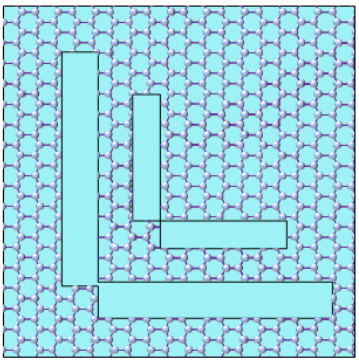

Figure 8. Graphene-based terahertz metamaterial polarization converter composed of graphene monolayer etched with pairs of rectangles [96].

2.2.2. Graphene-Based Multi-Functional Metamaterial Polarization Convention

Different from metamaterial absorbers, the graphene-based polarization converter can be used to achieve various functions in a single metamaterial structure. The polarization states of electromagnetic waves exhibit similar characteristics, and the amplitude and phase characteristics of different polarization states are relevant.

To achieve multi-functional metamaterial structures, most of the previously reported graphene-based metamaterial structures are used to achieve the LTC and LTL functions simultaneously [105–114]. These metamaterial structures can realize multi-frequency or broad-band LTL and LTC polarization conversion in a single metamaterial device. The quarter-wave plate (QWP) and a half-wave plate (HWP) can be constructed using the above-mentioned metamaterial structure. For example, in 2020, Y. Zhang et al. proposed a graphene-assisted switchable multi-functional metamaterial structure composed of metal strips placed on the polymer layer embedded with a nonstructured graphene film to manipulate the polarization characteristics of terahertz waves by external voltage [106]. The designed structure can be used as an adjustable QWP and HWP for both linearly and circularly polarized incident terahertz waves.

In addition, some different functions have also been integrated into a single graphene-based metamaterial device. J. X. Zhao et al. designed a three-layered metal-graphene-metal terahertz metamaterial structure to construct the switchable linear asymmetric transmission and polarization conversion through tuning the Fermi energy of graphene [115]. M. Sajjad et al. used double slotted graphene structure to construct multi-functional metamaterial polarization converter [116]. The device can achieve LTC polarization conversion and circular to cross-polarization conversion. D. B. Chen et al. designed a switchable broad-band polarization converter consist of periodically patterned graphene split-rings [117]. By designing different geometrical parameters, a polarization beam splitter and a transmissive focusing metamaterial structure were realized.

There are two main types of graphene microstructures in the metamaterial structures that are commonly used to achieve multiple functions, including single-layer graphene microstructures (discrete graphene patterns and continuous microstructures) and multi-layer graphene microstructures.

For single-layer discrete graphene patterns, many classical structures, including graphene patches [118], cross double-ellipse graphene patch [107], cross-shaped graphene patch [109], graphene ribbons [110,115], graphene disk with a hollow rectangle [108], graphene split-ring resonator [117], and so on, are used to achieve the polarization conversion function. In this case, Z. Liu et al. demonstrated that a layer of ion-gel lies on the top of graphene layer to serve as a transparent spacer layer, forming high capacitive properties between the top metal gate contacts and the underlying layer of the graphene microstructures [117]. Many single-layer hybrid graphene-metal metamaterial structures are also treated to realize the polarization conversions. In Figure 9, J. R. Zhang et al. designed a dual-functional tunable broad-band polarization converter using the hybrid graphene-metal metamaterial structure composed of anisotropic double-split gold ring and complementary double-split graphene ring [111]. The design can be switched between QWP and HWP in the frequency range of 1.38–1.72 THz by electrically changing the Fermi energy.

In addition, some continuous graphene layers, including continuous graphene microstructures (π-shaped hollows [113], cross-shaped graphene patch [109], reflective etched L-shaped structures on graphene [105], and so on) and nonstructured graphene films [106,114], are used to achieve the polarization conversion functions. These structures can effectively reduce the difficulty of manufacturing and electric tuning to a certain extent. M. Amin et al. presented a graphene-assisted metamaterial structure with L-structured unit cells to realize highly asymmetric radiation from the plasma polaron surface currents, resulting in linear and circular dichroism [105]. The LTC and LTL polarization conversion can be achieved at 1.85–2.81 THz and at 2.04–2.53 THz bands, respectively. Y. Zhang et al. proposed a graphene-assisted switchable multi-functional metamaterial structure composed of metal strips placed on the polymer layer embedded with a nonstructured graphene film to manipulate the

polarization characteristics of terahertz waves by external voltage [106]. The designed structure can be used as an adjustable QWP and HWP for both linearly and circularly polarized incident terahertz waves. In general, the combination of nonstructured graphene layer with dielectric microstructure can provide an efficient method to construct tunable metamaterial structures with high efficiency and great flexibility since the high-contrast dielectric metamaterial exhibits greater flexibility in efficient operation compared to their plasma counterparts. S. N. Guan et al. proposed a hybrid nonstructured graphene film-dielectric metamaterial to be used a dual-functional polarization converter [114]. This device can be switched between a reflective HWP and a QWP using biasing voltage. Switching of the two functions is caused by the obvious dispersion of the orthogonal eigenmodes and the overlap of graphene and dielectric resonant modes.

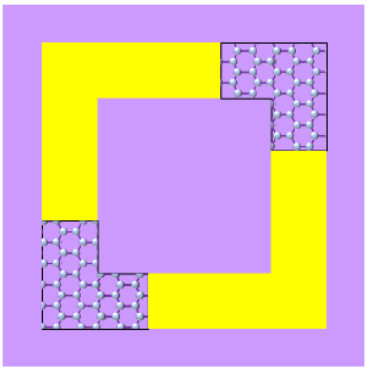

Figure 9. Metamaterial polarization converter structures based on double-split graphene ring [111].

The bandwidth of a metamaterial polarization converters can usually be improve based on the stack of multi-layer structures. In 2020, M. Sajjad et al. used double slotted graphene structure to enhance the bandwidth [116]. The proposed design can be used as an ultra broad-band (3.75–11.35 THz) LTL and CTC polarization converter with the PCR of 0.85. The bandwidth of the converter can be improved by increasing the graphene layers. In 2021, S. N. Guan et al. designed a reflective three-band metamaterial polarization converter consisting of an array of rectangular Si bars on a ten-layer graphene substrate [112]. The dynamical switch between the cross-linear polarization can cross-circular polarization can be achieved. Since it is no longer dependent on the plasma resonance in graphene, the reported hybrid metamaterial structure provides an alternative approach to construct switchable terahertz polarization converters with low stimuli voltage.

3. VO_2-Based Terahertz Metamaterial Absorber and Polarization Converter

Dynamical reconfigurable and switchable metamaterial structures based on phase change materials exhibit a controllable degree of freedom in the application of light-matter interaction and information processing [119]. Phase change materials, including GST [120–124], GeTe [125–127], VO_2 and so on, can be used to dynamically manipulate the metamaterial structures since the different optical and electronic characteristics of these materials can be achieved by changing their structural phases through a variety of external stimulation. As one of the phase change materials, VO_2 material demonstrates great application value in the field of reconfigurable structures [128–131]. At around 68 °C, the structure of VO_2 changes between the insulator monoclinic phase and the metal tetragonal phase. The phase transition is accompanied by significant variation in electrical and optical properties of VO_2. Different from graphene material, dynamic properties can by realized based on the reversible phase transition from insulator phase to metal phase by integrating the VO_2 material into the metamaterial structures. Several excitation methods, including thermal excitation [132], electrical excitation [133], and optical excitation [134], are usually treated to construct the VO_2-based reconfigurable metamaterial devices in practical applications, such as metamaterial memory [135], modulator [136], filter [137], and so on. The review of this part is classified

by the VO_2-based metamaterial structures to realize absorption, polarization conversion and multiple functions.

3.1. VO_2-Based Terahertz Metamaterial Absorber

Several VO_2-based structures are proposed to design metamaterial absorbers in terahertz region. One method to use VO_2 is that the VO_2 can be used as a part of the notch resonant rings or microstructures, and the structural characteristics can be changed by external stimulus [138,139]. In Figure 10a, T. T. Lv et al. designed a thermally adjustable terahertz metamaterial absorber containing a series of orthogonal coupled split-ring metal resonators with embedding VO_2 material in different gaps. The hybrid design and asymmetric VO_2 strips arrangement exhibit a novel concept for flexible adjustable of absorption bandwidth and dynamic range based on the external thermal stimulation. The broad-band absorption (−220 GHz bandwidth) and dual-band absorption can be realized with different states of VO_2 material [138]. Another method is to use VO_2 as a complete structure to achieve the absorption function, including I-shaped resonators [140], resonant rings [141–143], split-ring-resonators [144], nonstructured VO_2 film [145,146], and so on [147,148]. In Figure 10b, J. Huang et al. designed a tunable terahertz metamaterial absorber exhibiting two broad-band absorption characteristics [147]. The proposed design contains two VO_2 patterns. The high absorption about 80% can be achieved in the frequency bands of 0.56–1.44 THz and 2.88–3.65 THz. Absorption intensity can be changed from 20% to 90% by varying the conductivity of VO_2 through thermal stimulation. Our group designed a tunable terahertz metamaterial absorber with multi-defect combination embedded VO_2 thin film [146]. The absorption intensity at f = 4.08 THz and f = 4.33 THz are 99.8% and 99.9%, respectively. The phase transition of VO_2 can be controlled by changing ambient temperature, so that the absorption rates of two frequency points can be changed from 99.8% to 1.0%. A broad-band tunable metamaterial based on different radii of VO_2 rings in a single unit cell is proposed by B. Z. Cao et al. [141]. When VO_2 is in metal phase, the absorption above 90% has been achieved in the frequency band of 2.64–7 THz. When VO_2 is in insulator phase, the design can be regarded as a perfect reflector.

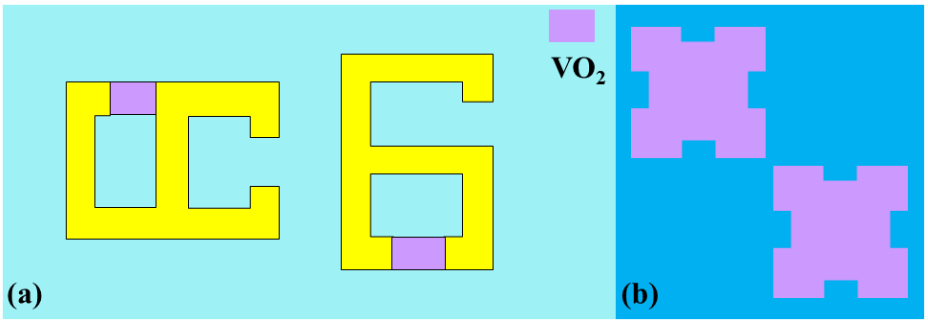

Figure 10. VO_2-based metamaterial absorber structures. (**a**) Split-ring metal resonators with embedded VO_2 material [138]; (**b**) two VO_2 patterns [147].

3.2. VO_2-Based Terahertz Metamaterial Polarization Converter

The VO_2-based metamaterial structures can be used to exhibit polarization conversion characteristics [149,150]. In 2019, J. Li et al. designed coding metasurfaces using VO_2 hybrid resonators for dynamically modulating terahertz waves, realizing the efficient modulation of the polarization and wavefront of the linearly and circularly polarized terahertz waves [149]. In 2021, F. Lv et al. designed a switchable chiral metamaterial structure to achieve asymmetric transmission polarization [150]. When VO_2 is in insulator state, the structure exhibits asymmetric transmission and the LTL polarization conversion in the frequency ranges of 1.67–1.74 THz and 1.86–2.05 THz with low ellipticity and high PCR (>90%). Two typical structures with circular- and square- split ring are given in Figure 11a,b.

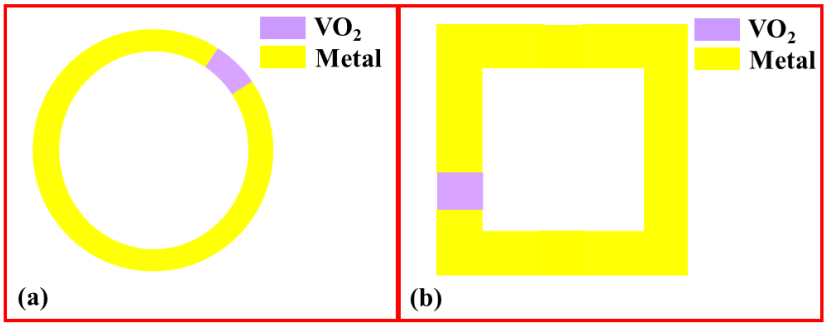

Figure 11. Metamaterial polarization converters based on (**a**) circular split ring resonator structure; (**b**) square split ring resonator structure.

3.3. VO_2-Based Terahertz Metamaterial Multi-Functional Structures

As described above, by changing the phase characteristics, VO_2 can exhibit two completely different states (insulator and metal), so that two or more functions can be realized in a single structure. VO_2-based metamaterial structures can perform absorption functions with different characteristics [151]. In 2020, Z. Y. Song et al. used the phase-transition characteristic of VO_2 to design a multi-layer hybrid metamaterial with a switchable behavior between broad-band absorption and narrow-band absorption [151]. The structure is illustrated in Figure 12. When VO_2 is in metal state, a broad-band frequency region of 0.393–0.897 THz with the absorption above 90% has been obtained. When VO_2 is in insulator state, the designed structure can be used as a narrow-band absorber at the frequency of 0.677 THz.

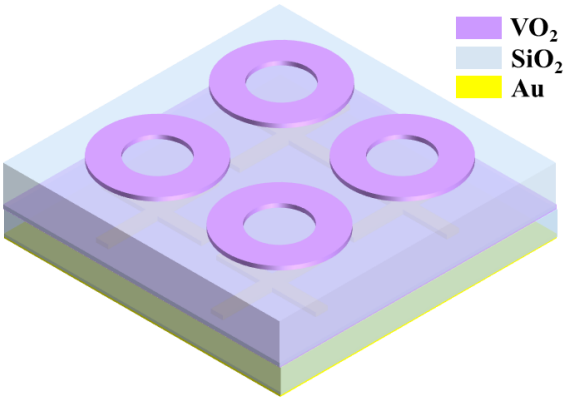

Figure 12. VO_2-based broad-band absorption and narrow-band absorption structure [151].

The absorption and polarization conversion can also be obtained in a single metamaterial structure by using the insulator-to-metal phase transition of VO_2-based metamaterial structures in terahertz region [152,153]. In Figure 13a, Z. Y. Song et al. presented a dual-functional design to realize the broad-band absorption and polarization conversion using a tunable VO_2-assisted metamaterial structure [152]. When VO_2 is in metal state, the proposed tunable metamaterial structure behaves as a broad-band absorber with the absorption above 90% in the range of 0.52–1.2 THz. When VO_2 is in insulator state, a terahertz LTL polarization converter with the efficiency of 90% in the frequency band of 0.42–1.04 THz is achieved based on a simple anisotropic metamaterial structure. We proposed a switchable terahertz metamaterial structure to realize the transform between the broad-band absorption and LTC polarization conversion by treating the phase transition of VO_2 [153]. As depicted in Figure 13b, a VO_2 square ring and a nonstructured VO_2 film are used in the structure. At high temperature, the device can function as a broad-band absorber with a high absorption (>90%) in 0.74–1.62 THz. At room temperature, the device functions as a broad-band LTC polarization converter in 1.47–2.27 THz.

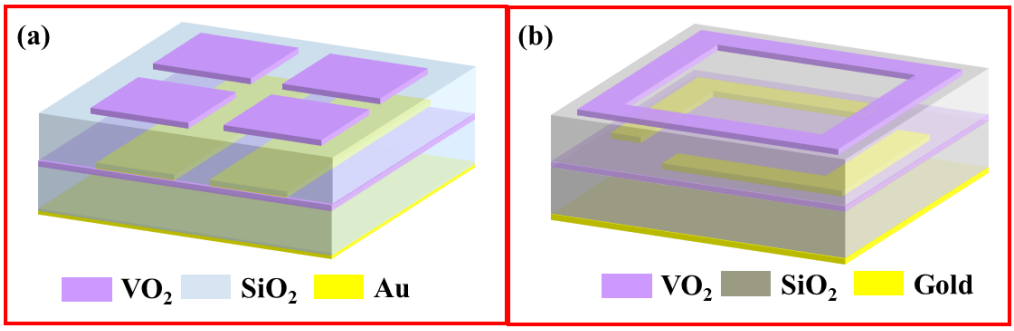

Figure 13. VO_2-based metamaterial structures realizing absorption and polarization. (**a**) Proposed by Z. Y. Song et al. [152]. (**b**) Proposed by our group [153].

Dynamically switchable half-/quarter-wave plates based on the phase transition of VO_2 material have recently been investigated [154–156]. In 2020, J. Luo et al. proposed a metal-VO_2 metamaterial structure with broad-band and functionally tunable polarization conversion [154]. A nonstructured VO_2 film is used in the design. The designed structure can be switched between a HWP and a QWP in a broad-band frequency range of 0.66–1.40 THz with a relative bandwidth of 71.8%. The VO_2-metal hybrid metamaterial for obtaining broad-band dynamically tunable half-/quarter-wave plate using the transition from the overdamped to the underdamped resonance [155]. By changing the VO_2 conductivity, the structure can be switched between a HWP with PCR above 96% and a QWP with ellipticity close to -1 in the broad-band frequency range of 0.8–1.2 THz. In Figure 14, very recently, we designed a reflective dual-functional terahertz metamaterial structure realizing LTL and LTC polarization conversion based on the phase transition of nonstructured VO_2 film [156]. When VO_2 film is in insulator state, the PCR of the LTL converter is higher than 0.9 in the range of 0.912 to 2.146 THz. When VO_2 film is in metal state, the ellipticity of the LTC converter is close to -1, while the axis ratio is lower than 3 dB in the range of 1.07–1.67 THz.

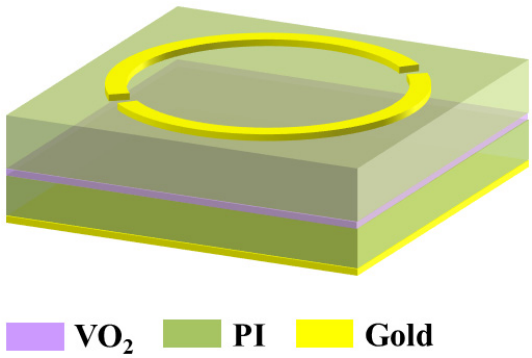

Figure 14. Nonstructured VO_2 film-based metamaterial multi-functional polarization structure. Adapted with permission from Ref. [156], 2022, Copyright the author.

Due to the dielectric properties of the VO_2 with insulating state, transmission function combined with other functions can also be realized [119,157–159]. In Figure 15a, L. L. Chen et al. introduced VO_2 film into a multi-layer design to achieve the dual-function of absorption and high transmission [157]. When VO_2 is in metal state, the proposed structure exhibits high absorption results from localized magnetic resonance. When VO_2 is in insulator state, the proposed structure can be used as a transparent conducting metal. In 2020, J. S. Schalch et al. designed an electrically actuated, broad-band terahertz switch, which can be transformed from the transparent state with low reflection to the absorption state suppressing the reflection and transmission [158]. The structure is integrated with a nonstructured VO_2 film performing the insulator-metal-transition. The terahertz time-domain spectroscopy measurement results demonstrate that a broad bandwidth of 700 GHz

amplitude modulation with suppressed reflection and above 90% transmission can be achieved. In Figure 15b, C. X. Liu et al. proposed a terahertz metamaterial structure to realize the functions of optical buffering and absorption based on a phase-change VO_2 film [159]. When VO_2 is in insulator state, a significant delay can be observed when the incident pulses pass through the proposed structure. Once the VO_2 film is switched to the metal state, the proposed structure can be used as a terahertz absorber with a maximum absorption intensity of 94% at 1.04 THz.

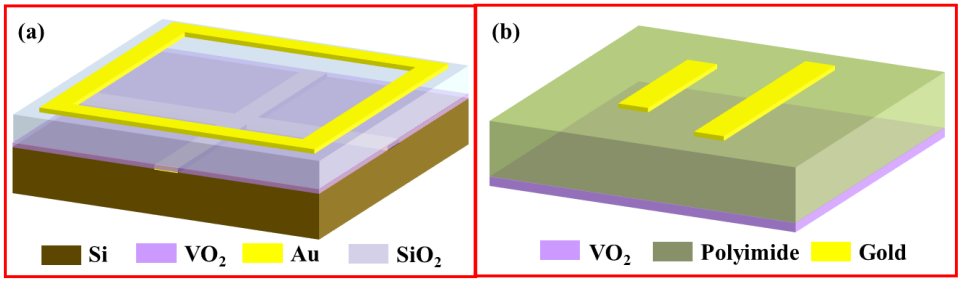

Figure 15. VO_2-based transmissive metamaterial structures. (**a**) Structure designed by L. L. Chen et al. [157]; (**b**) structure designed by C. X. Liu et al. [159].

4. Dirac Semimetal-Based Terahertz Metamaterial Absorber and Polarization Converter

As a three-dimensional (3D) analogy of graphene, Dirac semimetal (DSM) not only provides the advantages of 2D material as photosensitive materials, but also has more significant advantages than graphene in resisting environmental defects or excessive conductive bulk states [160–162]. Since the crystalline symmetry protection of DSM prevents the formation of gaps [163–165], the carrier mobility can reach 9×10^6 $cm^2V^{-1}s^{-1}$ [166], which is much larger than the value of graphene [26]. The dynamical change of the DSM conductivity can be realized by tuning the Fermi energy through alkaline surface doping [167,168]. Similar to graphene, the Fermi energy and relative permittivity of DSMs can also be dynamically changed using the external electric stimulation [169]. These properties ensure that DSMs can be used as a novel material to tune the frequencies and will exhibit great potential in photovoltaic devices, sensor, imaging, and communications [162]. Furthermore, DSM shows metallic characteristics when frequency is below Fermi energy and will show dielectric characteristics when frequencies is above Fermi energy [170]. The resonant frequency is mainly influenced by the real part of the permittivity, and the loss is influenced by the imaginary part [169]. The review of this part is classified by the DSM-based metamaterial structures to realize absorption, polarization conversion and multiple functions.

4.1. DSM-Based Terahertz Metamaterial Absorber

At terahertz frequency region, the DSM materials with metallic properties can be used as a Salisbury screen to construct absorbers more conveniently than graphene [162,171–173]. In Figure 16a, G. D. Liu et al. designed a bulk DSM-based tunable narrow-band terahertz metamaterial absorber [172]. The structure contains photonic slabs with a thick DSM film. The resonant frequency peak can be shifted from 1.381 THz to 1.395 THz with the absorption higher than 95% by adjusting the Fermi energy of DSM. Additionally, the narrow-band characteristic may be caused by the low power loss of guided mode resonance in the dielectric layer. A tunable triple narrow-band perfect absorber is proposed based on a square harmonic oscillator array containing four bulk DSM thin films and a DSM square ring [171]. The absorber can provide high absorption higher than 0.96 at 2.14 THz, 1.83 THz and 1.21 THz. The molecular perturbation theory has been used to confirm the mechanism of the absorber. The perturbation theory function can be treated to estimate the variation of the absorber resonant frequency since the material perturbation in the best films. As demonstrated in Figure 16b, another three-band terahertz metamaterial absorber treating a

nonstructured bulk DSM film layer is designed [173]. Three absorption peaks at 0.80 THz, 1.72 THz and 3.38 THz with high absorption (>99.4%) are obtained. By adjusting the Fermi energy of the DSM film, the absorption peaks can be changed.

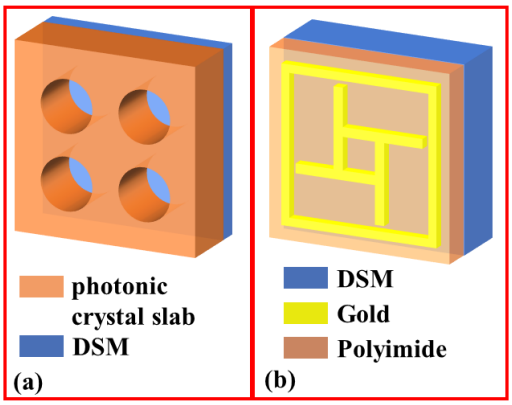

Figure 16. DSM-based metamaterial absorbers. (**a**) Photonic slabs with a thick DSM film [172]; (**b**) bulk DSM film layer [173].

4.2. DSM-Based Terahertz Polarization Converter

In addition, DSM-based metamaterial structures can be used to construct terahertz polarization converter [174]. In 2019, L. L. Dai et al. proposed a DSM-based metamaterial structure featuring tunable and broad-band terahertz LTL polarization conversion in transmissive mode [174]. The single-layer DSM microstructure consists of two rotationally symmetric 'E' structures connected by a center line which are subtracted from the bulk DSM layer on top of the silicon dioxide (SiO_2) layer. In the frequency range of 3.82–7.88 THz, the PCR almost keeps above 80%. The operation properties can be manipulated by tuning the Fermi energy of the bulk DSM. Figure 17 shows the typical two rotationally symmetric 'E' shapes.

Figure 17. Two rotationally symmetric 'E' shapes.

4.3. DSM-Based Terahertz Metamaterial Multi-Functional Structure

Although absorption- and polarization-related metamaterial structures have been broadly investigated, they only perform independent single functions. A DSM-based terahertz metamaterial structure that features multiple functions in a single metamaterial structure is more popular [175]. A three-layer complementary strip DSM metamaterial structure is designed by L. L. Dai et al. to realize polarization rotation, polarization conversion and asymmetric transmission [175]. The polarization angle of linearly polarized wave can be rotated from 0° to 90° in 1.3–1.63 THz. For realizing the asymmetric transmission, the polarization conversion efficiency is above 98% and the asymmetric transmission parameter is above 50% in 1.3–1.63 THz.

5. Combination of Different Functional Materials

Based on the VO_2 transition from an insulator dielectric state to a metal state and the tunable of DSM Fermi energy, several multi-functional metamaterial structures are designed to integrate different functions into a single metamaterial structure, including LTL and LTC polarization converter [176], asymmetric transmission and dual-directional absorption [177], polarization conversion and reflection device [178], different absorption characteristics [19], and so on. In Figure 18a, Y. P. Zhang et al. designed a dual-function metamaterial structure treating DSM and VO_2 material [176]. When VO_2 is in insulator state, the structure can be used as an asymmetric transmission device to realize a broad-band LTL polarization conversion with the PCR reaches 99% in 2.023–5.971 THz. When VO_2 is in metal state, the structure can be used as a reflective device to realize broad-band LTC polarization conversion and linear polarization conversion at 4.053 THz. In Figure 18b, T. L. Wang et al. designed a switchable dual-functional terahertz metamaterial structure treating DSM films and VO_2 [177]. The switch between the dual-functional asymmetric transmission and two-directional absorption can be achieved based on the insulator-to-metal phase transition of VO_2 in the terahertz region. In each case, the operation characteristics can be adjusted by changing the Fermi energy of the DSM. In Figure 18c, C. H. Yang et al. presented a dual-functional polarization converter using the combination of DSMs and VO_2 [178]. The design contains four parts: two DSM layers, a loss-free benzocyclobutene (BCB) layer, a copper grating, and a VO_2 film. The resonant frequency can be dynamically adjusted by changing the Fermi energy of the DSMs. When VO_2 is in insulator state, the design exhibits the transmissive polarization conversion. When VO_2 is in metallic state, the proposed structure shows the reflective function maintaining efficient circular polarized wave chirality in a broad range. A switchable metamaterial absorber with three-band and broad-band properties treating the combination of DSM and VO_2 has been reported [19]. By changing the phase state of VO_2, the absorber presents three distinctive absorption peaks with absorption >98% (insulator state) and broad-band absorption (metal state). Since the tunable Fermi energy of DSM, resonant frequencies can be dynamically adjusted. The proposed design solution combines the bulk DSMs and VO_2, which not only opens up a novel method for the realization of a switchable absorber from three-band to wide-band absorption, but also for the control of the resonant frequency and absorption amplitude in terahertz region.

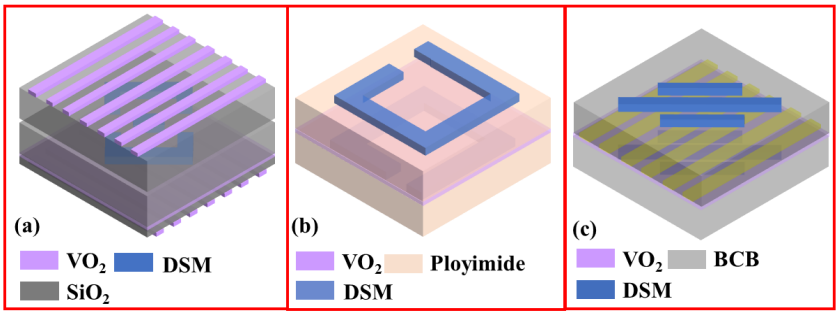

Figure 18. Multi-functional metamaterial structures based on the combination of VO_2 and DSM. (**a**) LTL and LTC polarization converter [176]; (**b**) asymmetric transmission and dual-directional absorption [177]; (**c**) polarization conversion and reflection device [178].

By treating the manipulated characteristics through Fermi energy of graphene and the phase transition characteristics of VO_2, some switchable multi-functional metamaterial structures can be constructed to realize different functions in a single metamaterial structure, including absorption with different characteristics [179–186], reflection and absorption [187,188], absorption and polarization conversion [189], and so on. In Figure 19a, H. L. Zhu et al. designed a tunable metamaterial structure to realize the broad-band and multi-band absorption treating the combination of graphene and VO_2 [179]. The switchable functions can be realized depend on the phase transition of VO_2. When VO_2 is in insulator

state, the structure provides high absorption (>90%) in a broad-band range of 1.06–2.58 THz. When VO_2 is in metal state, the structure exhibits a three-band absorption at the frequencies of 1 THz, 2.45 THz and 2.82 THz. In addition, by tuning the Fermi energy of the graphene, the absorption bandwidth, intensity, and resonant frequencies can be adjusted. A tunable dual-functional metamaterial structure realizing terahertz anomalous reflection and broad-band absorption based on the combination of graphene and VO_2 has been reported by Z. K. Zhou et al. [187]. The structure contains six layers of different materials. The top layer is VO_2 patch. The middle layer contains Topas layer, VO_2 film, graphene microstructure, and Topas layer. The bottom layer is a gold film. When the phase of VO_2 varies from metal to insulator, the metamaterial structure can be switched from an anomalous reflector to a broad-band absorber. Additionally, the change of graphene Fermi energy can be used to adjust the absorption bandwidth and efficiency. In Figure 19b, a metamaterial structure has been designed to provide absorption and polarization conversion functions by treating the dielectric metasurface composed of VO_2 and graphene array [189]. When temperature is high (340 K), the structure provides the absorption function and the absorption intensity can be controlled by the variation of temperature. At room temperature, the structure can be used as a polarization converter, and the characteristics can be adjusted by changing the voltage applied on the graphene.

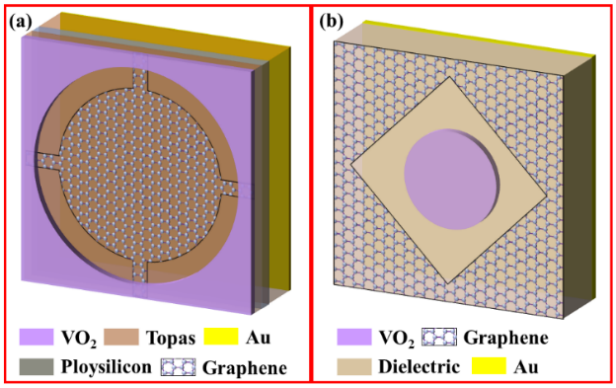

Figure 19. Multi-functional metamaterial structures based on the combination of VO_2 and graphene. (**a**) Realizing absorption with different characteristics [179]; (**b**) realizing absorption and polarization conversion [189].

Utilizing the properties of graphene and DSM, several metamaterial structures based on the combination of them exhibit switchable characteristics by modulating the Fermi energy of graphene and DSM material, resulting in the design of absorbers [169,190,191]. H. Xiong et al. designed a dual-controlled broad-band terahertz metamaterial absorber by integrating graphene and DSM into a single structure [169]. As shown in Figure 20, the structure contains a graphene microstructure, a bulk DSM microstructure, Al_2O_3 layer, and a gold background. The high absorption (>90%) can be realized in a wide frequency band of 4.79–8.99 THz. The control of the absorption characteristics can be achieved independently or jointly by changing the Fermi energy of graphene or DSM rather than reconstructing the structure.

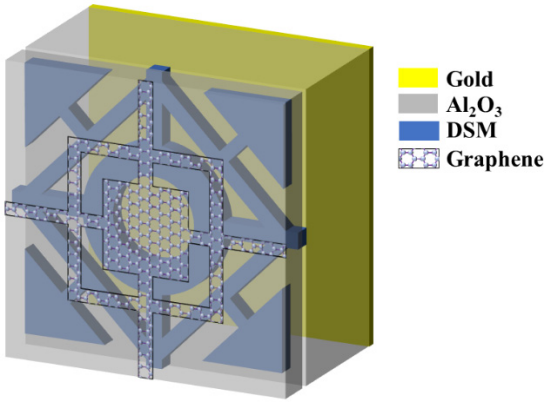

Figure 20. Designed absorber based on the combination of DSM and graphene [169].

6. Conclusions and Perspectives

In this topical review, we briefly reviewed the recent researches about functional materials-assisted metamaterial structures with switchable manipulation by external stimulations, focusing mainly on the terahertz metamaterial absorbers and polarization converters with different operation characteristics. We expatiated on the three functional materials including graphene, VO_2, and DSM. For graphene materials, terahertz metamaterial absorbers and polarization converters are usually constructed with single-layer and multi-layer graphene microstructures. Graphene can be designed as discrete microstructures, continuous microstructures, or even nonstructured graphene films in the unit cells. By tuning the Fermi energy of graphene, the absorption and polarization conversion characteristics can be dynamically tuned. For VO_2 materials, they are usually designed as a part of notch resonant rings or microstructures and as separate whole microstructures to construct the terahertz metamaterial absorbers and polarization converters. Different from graphene materials, since the VO_2 exhibits insulator-to-metal transition characteristic, it will undergo a transition from the metallic state to an insulator state under various external field stimulations. Therefore, a single metamaterial structure based on VO_2 material can be used to switch between different functions. As well as providing more freedom for designing metamaterial structures, the DSM is easier to use than graphene and compatible with current semiconductor manufacturing processes. The DSMs-based terahertz metamaterial structures provide a wonderful platform to design absorbers and polarization converters. Moreover, novel dynamical switchable metamaterial structures based on the combination of two different functional materials have also been discussed. Related researchers can find the most suitable structures and functional materials and integrate them into the single unit cell to design metamaterial functional devices. This topical review can serve as a useful guide for researchers to investigate the functional materials-assisted metamaterial structures, not limited to absorbers and polarization converters.

Despite excellent achievements have been obtained by treating metamaterial structures and functional materials, there is still space for further improvement in the related field to achieve novel functional materials-assisted metamaterial structures in place of traditional optical elements, which in turn causes new challenges to the exploration of structure design and functional materials selection. Some recently emerged mechanisms and novel materials, which enable metamaterials devices, including bound states in the continuum [192], 2D α-phase molybdenum trioxides (α-MoO_3) [193,194], Ti nanorings [195], c-Si/ZnO Heterojunction ultrathin-film [196], and so on. Great technical challenges still exist, because some theoretically proven ideas are too complicated to be fabricated and are limited by existing manufacturing technologies. In terahertz frequency band, the functional materials-based metamaterial structure processing and nanoscale patterning resolution may be practically realized based on the multi-step fabrication and costly focused ion beam or electron beam lithography technologies [2,197]. In addition, further efforts should be made to bridge the gap between high efficiency in large processing areas and low

cost. At present, the experimental realization of functional materials-assisted metamaterial structures mainly relies on expensive manufacturing methods, which are not suitable for mass production. Lastly, achieving small devices sizes at terahertz frequency band and conquering small effects at the nanoscale should be considered. On the one hand, reducing the size of resonator of the metamaterial structures when operating at terahertz frequency is a requirement for compact integrated circuits and new generation communication systems. On the other hand, when metamaterial microstructures exhibit nano-scale size, the physical characteristics, including melting point, oxidation, grain boundary effect, and so on, are different, resulting in the complicated designs.

In addition to the functional materials-based metamaterial structures summarized in this paper, we should bear in mind that we can integrate other various functional materials into the metamaterial structures to construct excellent dynamical switchable devices in terahertz frequency band, not limited to absorbers and polarization converters. In general, despite the daunting challenges, the rapid expansion of research into functional materials-based metamaterial structures demonstrate the great potential in the related researches. Furthermore, the switchable and versatile applications will promote the above-mentioned devices, which will be adopted by the experimental research in the near future.

Author Contributions: Conceptualization, D.Y.; software, J.L. (Jining Li); investigation, G.Q., Y.Q. and Q.F.; resources, Y.W. and J.L. (Jining Li); writing—original draft preparation, D.Y.; writing—review and editing, X.L. and J.L. (Jiusheng Li). All authors have read and agreed to the published version of the manuscript.

Funding: This research was funded by Fundamental Research Funds for the Provincial Universities of Zhejiang (2021YW13); National Natural Science Foundation of China (62001444); State's Key Project of Research and Development Plan for National Quality Infrastructure (2021YFF0600300); Natural Science Foundation of Zhejiang Province (LQ20F010009, LGF19F010003). Research Fund of The State Key Laboratory of Coal Resources and safe Mining, CUMT (SKLCRSM21KF010).

Data Availability Statement: Not applicable.

Conflicts of Interest: The authors declare no conflict of interest.

References

1. Cheng, J.; Fan, F.; Chang, S. Recent progress on graphene-functionalized metasurfaces for tunable phase and polarization control. *Nanomaterials* **2019**, *9*, 398. [CrossRef] [PubMed]
2. Xiao, S.Y.; Wang, T.; Liu, T.T.; Zhou, C.B.; Jiang, X.Y.; Zhang, J.F. Active metamaterials and metadevices: A review. *J. Phys. D Appl. Phys.* **2020**, *53*, 503002. [CrossRef]
3. Liu, Z.H.; Li, X.J.; Yin, J.; Hong, Z. Asymmetric all Silicon micro-antenna array for high angle beam bending in terahertz band. *IEEE Photonics J.* **2019**, *11*, 5900509. [CrossRef]
4. Li, X.J.; Liu, Z.H.; Yan, D.X.; Li, J.N.; Li, J.S.; Qiu, G.H.; Hou, X.M.; Cheng, G. Experimental demonstration of 3D printed terahertz polarization-insensitive flat devices based on low-index meta-gratings. *J. Phys. D Appl. Phys.* **2020**, *53*, 505301. [CrossRef]
5. Zhao, X.L.; Yuan, C.; Lv, W.H.; Xu, S.L.; Yao, J.Q. Plasmon-Induced Transparency in Metamaterial Based on Graphene and Split-Ring Resonators. *IEEE Photonics Tech. Lett.* **2015**, *27*, 1321–1324. [CrossRef]
6. Chen, H.; Chen, Z.; Yang, H.; Wen, L.; Yi, Z.; Zhou, Z.; Dai, B.; Zhang, J.; Wu, X.; Wu, P. Multi-mode surface plasmon resonance absorber based on dart-type single-layer graphene. *RSC Adv.* **2022**, *12*, 7821–7829. [CrossRef]
7. Yang, T.; Liu, X.M.; Wang, C.; Liu, Z.T.; Sun, J.B.; Zhou, J. Polarization conversion in terahertz planar metamaterial composed of split-ring resonators. *Opt. Commun.* **2020**, *472*, 125897. [CrossRef]
8. Landy, N.I.; Sajuyigbe, S.; Mock, J.; Smith, D.; Padilla, W. Perfect metamaterial absorber. *Phys. Rev. Lett.* **2008**, *100*, 207402. [CrossRef]
9. Hao, J.M.; Wang, J.; Liu, X.L.; Padilla, W.J.; Zhou, L.; Qiu, M. High performance optical absorber based on a plasmonic metamaterial. *Appl. Phys. Lett.* **2010**, *96*, 251104. [CrossRef]
10. Lapine, M.; Powell, D.; Gorkunov, M.; Shadrivov, I.; Marqu'es, R.; Kivshar, Y. Structural tunability in metamaterials. *Appl. Phys. Lett.* **2009**, *95*, 084105. [CrossRef]
11. Tao, H.; Strikwerda, A.; Fan, K.; Padilla, W.J.; Zhang, X.; Averitt, R.D. Reconfigurable Terahertz Metamaterials. *Phys. Rev. Lett.* **2009**, *103*, 147401. [CrossRef] [PubMed]
12. Zhu, W.M.; Liu, A.Q.; Zhang, X.M.; Tsai, D.P.; Bourouina, T.; Teng, J.H.; Zhang, X.H.; Guo, H.C.; Tanoto, H.; Mei, T.; et al. Switchable Magnetic Metamaterials Using Micromachining Processes. *Adv. Mater.* **2011**, *23*, 1792–1796. [CrossRef] [PubMed]

13. Lapine, M.; Shadrivov, I.V.; Powell, D.A.; Kivshar, Y.S. Magnetoelastic metamaterials. *Nat. Mater.* **2012**, *11*, 30–33. [CrossRef] [PubMed]
14. Valente, J.; Ou, J.Y.; Plum, E.; Youngs, I.J.; Zheludev, N.I. Reconfiguring photonic metamaterials with currents and magnetic fields. *Appl. Phys. Lett.* **2015**, *106*, 111905. [CrossRef]
15. Wang, L.; Xiao, R.-W.; Ge, S.-J.; Shen, Z.-X.; Lü, P.; Hu, W.; Lu, Y.-Q. Research progress of terahertz liquid crystal materials and devices. *Acta Phys. Sin.* **2019**, *68*, 084205. [CrossRef]
16. He, Z.H.; Lu, H.; Zhao, J.L. Polarization independent and non-reciprocal absorption in multi-layer anisotropic black phosphorus metamaterials. *Opt. Express* **2021**, *29*, 21336–21347. [CrossRef]
17. Li, Y.; Wang, S.Y.; Ou, Y.H.; He, G.L.; Zhai, X.; Lim, H.J.; Wang, L.L. Dynamically tunable narrowband anisotropic total absorption in monolayer black phosphorus based on critical coupling. *Opt. Express* **2021**, *29*, 2909–2919. [CrossRef]
18. He, X.Y.; Liu, F.; Lin, F.T.; Shi, W.Z. Tunable terahertz Dirac semimetals metamaterials. *J. Phys. D Appl. Phys.* **2021**, *54*, 235103. [CrossRef]
19. Ban, S.H.; Meng, H.Y.; Zhai, X.; Xue, X.X.; Lin, Q.; Li, H.J.; Wang, L.L. Tunable triple-band and broad-band convertible metamaterial absorber with bulk Dirac semimetal and vanadium dioxide. *J. Phys. D Appl. Phys.* **2021**, *54*, 174001. [CrossRef]
20. Liu, C.; Bai, Y.; Zhou, J.; Zhao, Q.; Qiao, L. A Review of Graphene Plasmons and its Combination with Metasurface. *J. Korean Ceram. Soc.* **2017**, *54*, 349–365. [CrossRef]
21. Nemati, A.; Wang, Q.; Hong, M.; Teng, J. Tunable and reconfigurable metasurfaces and metadevices. *Opto-Electron. Adv.* **2018**, *1*, 180009. [CrossRef]
22. Novoselov, K.S.; Fal, V.I.; Colombo, L.; Gellert, P.R.; Schwab, M.G.; Kim, K. A roadmap for graphene. *Nature* **2012**, *490*, 192–200. [CrossRef] [PubMed]
23. Geim, A.K.; Novoselov, K.S. The rise of graphene. *Nat. Mater.* **2007**, *6*, 183–191.
24. Zamzam, P.; Rezaei, P.; Khatami, S.A. Quad-band polarization-insensitive metamaterial perfect absorber based on bilayer graphene metasurface. *Phys. E Low-Dimens. Syst. Nanostruct.* **2021**, *128*, 114621. [CrossRef]
25. Zhang, E.L.; Zhou, Q.; Shen, J. Resistive switching device based on highmobility graphene and its switching mechanism. *J. Phys. Conf. Seri.* **2019**, *1168*, 022074. [CrossRef]
26. Bolotin, K.I.; Sikes, K.J.; Jiang, Z.; Klima, M.; Fudenberge, G.; Hone, J.; Kim, P.; Stormer, H.L. Ultrahigh electron mobility in suspended graphene. *Solid State Commun.* **2008**, *146*, 351–355. [CrossRef]
27. Banszerus, L.; Schmitz, M.; Engels, S.; Dauber, J.; Oellers, M.; Haupt, F.; Watanabe, K.; Taniguchi, T.; Beschoten, B.; Stampfer, C. Ultrahigh-mobility graphene devices from chemical vapor deposition on reusable copper. *Sci. Adv.* **2015**, *1*, e1500222. [CrossRef]
28. Papasimakis, N.; Luo, Z.Q.; Shen, Z.X.; Angelis, F.D.; Fabrizio, E.D.; Nikolaenko, A.E.; Zheludev, N.I. Graphene in a photonic metamaterial. *Opt. Express* **2010**, *18*, 8353–8359. [CrossRef]
29. Huang, Y.Y.; Yao, Z.H.; Hu, F.R.; Wang, Q.; Yu, L.L.; Xu, X.L. Manipulating magnetoinductive coupling with graphene-based plasmonic metamaterials in THz region. *Plasmonics* **2006**, *11*, 963–970. [CrossRef]
30. Xiong, H.; Jiang, Y.N.; Yang, C.; Zeng, X.P. Frequency-tunable terahertz absorber with wire-based metamaterial and graphene. *J. Phys. D Appl. Phys.* **2017**, *51*, 015102. [CrossRef]
31. He, X.J.; Yao, Y.; Zhu, Z.H.; Chen, M.H.; Zhu, L.; Yang, W.L.; Yang, Y.Q.; Wu, F.M.; Jiang, J.X. Active graphene metamaterial absorber for terahertz absorption bandwidth, intensity and frequency control. *Opt. Mater. Express* **2018**, *8*, 1031–1042. [CrossRef]
32. Yi, Z.; Chen, J.J.; Cen, C.L.; Chen, X.F.; Zhou, Z.G.; Tang, Y.J.; Ye, X.; Xiao, S.; Luo, W.; Wu, P. Tunable graphene-based plasmonic perfect metamaterial absorber in the THz region. *Micromachines* **2019**, *10*, 194. [CrossRef] [PubMed]
33. Yan, D.X.; Li, J.S. Tunable all-graphene-dielectric single-band terahertz wave absorber. *J. Phys. D Appl. Phys.* **2019**, *52*, 275102. [CrossRef]
34. Yao, G.; Ling, F.R.; Yue, J.; Luo, C.Y.; Yao, J.Q. Dual-band tunable perfect metamaterial absorber in the THz range. *Opt. Express* **2016**, *24*, 1518–1527. [CrossRef] [PubMed]
35. Su, Z.P.; Wang, Y.K.; Luo, X.; Luo, H.; Zhang, C.; Li, M.X.; Sang, T.; Yang, G.F. A tunable THz absorber consisting of an elliptical graphene disk array. *Phys. Chem. Chem. Phys.* **2018**, *20*, 14357–14361. [CrossRef] [PubMed]
36. Yi, Z.; Lin, H.; Niu, G.; Chen, X.F.; Zhou, Z.G.; Ye, X.; Duan, T.; Yi, Y.; Tang, Y.; Yi, Y. Graphene-based tunable triple-band plasmonic perfect metamaterial absorber with good angle-polarization-tolerance. *Results Phys.* **2019**, *13*, 102149. [CrossRef]
37. Zhang, X.M.; Wu, W.W.; Li, C.X.; Wang, C.; Ma, Y.H.; Yang, Z.B.; Sun, G.; Yuan, N.C. A dual-band terahertz absorber with two passbands based on periodic patterned graphene. *Materials* **2019**, *12*, 3016. [CrossRef]
38. Zhang, L.H.; Hu, F.R.; Xu, X.L.; Wang, Y.E.; Guo, E.Z. Design of separately tunable terahertz two-peak absorber based on graphene. *Opt. Commun.* **2016**, *369*, 65–71. [CrossRef]
39. Huang, M.; Cheng, Y.; Cheng, Z.; Chen, H.; Mao, X.; Gong, R. Based on graphene tunable dual-band terahertz metamaterial absorber with wide-angle. *Opt. Commun.* **2018**, *415*, 194–201. [CrossRef]
40. Nejat, M.; Nozhat, N. Sensing and switching capabilities of a graphene-based perfect dual-band metamaterial absorber with analytical methods. *J. Opt. Soc. Am. B* **2020**, *37*, 1359–1366. [CrossRef]
41. Xu, K.D.; Li, J.X.; Zhang, A.X.; Chen, Q. Tunable multi-band terahertz absorber using a single-layer square graphene ring structure with T-shaped graphene strips. *Opt. Express* **2020**, *28*, 11482–11492. [CrossRef] [PubMed]
42. Xu, K.D.; Cai, Y.; Cao, X.; Guo, Y.; Zhang, Y.; Chen, Q. 2020 Multi-band terahertz absorbers using T-shaped slot-patterned graphene and its complementary structure. *J. Opt. Soc. Am. B* **2020**, *37*, 3034–3040. [CrossRef]

43. Wang, F.L.; Huang, S.; Li, L.; Chen, W.D.; Xie, Z.W. Dual-band tunable perfect metamaterial absorber based on graphene. *Appl. Opt.* **2018**, *57*, 6916–6922. [CrossRef] [PubMed]
44. Qing, Y.M.; Ma, H.F.; Yu, S.; Cui, T.J. Tunable dual-band perfect metamaterial absorber based on a graphene-SiC hybrid system by multiple resonance modes. *J. Phys. D Appl. Phys.* **2018**, *52*, 015104. [CrossRef]
45. Gao, E.; Liu, Z.; Li, H.; Xu, H.; Zhang, Z.; Luo, X.; Xiong, C.; Liu, C.; Zhang, H.; Zhou, F. Dynamically tunable dual plasmon-induced transparency and absorption based on a single-layer patterned graphene metamaterial. *Opt. Express* **2019**, *27*, 13884–13894. [CrossRef] [PubMed]
46. Li, J.; Liao, Q.; Li, H.; Yu, T.; Wang, T. Tunable dual-band perfect metamaterial absorber based on monolayer graphene arrays as refractive index sensor. *Jpn. J. Appl. Phys.* **2020**, *59*, 095002. [CrossRef]
47. Liu, Z.Y.; Li, J.; He, L.J.; Yu, T.B. Graphene-based dual-band tunable perfect absorber in THz range. *J. Mod. Opt.* **2021**, *68*, 93–99. [CrossRef]
48. Xiang, Y.; Wang, L.; Lin, Q.; Xia, S.; Qin, M.; Zhai, X. Tunable dual-band perfect absorber based on L-shaped graphene resonator. *IEEE Photonics Tech. Lett.* **2019**, *31*, 483–486. [CrossRef]
49. Lu, Z.H.; Yang, Y.G.; Huang, J.L. Dual-band terahertz metamaterial absorber using hexagon graphene structure. *Microw. Opt. Techn. Lett.* **2021**, *63*, 1797–1802. [CrossRef]
50. Zhao, Y.; Wu, B.; Huang, B.; Cheng, Q. Switchable broadband terahertz absorber/reflector enabled by hybrid graphene-gold metasurface. *Opt. Express* **2017**, *25*, 7161–7169. [CrossRef]
51. Yan, D.X.; Li, J.S. Tuning control of dual-band terahertz perfect absorber based on graphene single layer. *Laser Phys.* **2019**, *29*, 046203. [CrossRef]
52. Luo, H.; Shangguan, Q.Y.; Yi, Y.T.; Cheng, S.B.; Yi, Y.G.; Li, Z. Tunable "Ancient Coin"-Type Perfect Absorber with High Refractive Index Sensitivity and Good Angular Polarization Tolerance. *Coatings* **2021**, *11*, 814. [CrossRef]
53. Li, J.S.; Sun, J.Z. Umbrella-shaped graphene/Si for multi-band tunable terahertz absorber. *Appl. Phys. B* **2019**, *125*, 183. [CrossRef]
54. Li, J.S.; Yan, D.X.; Sun, J.Z. Flexible dual-band all-graphene-dielectric terahertz absorber. *Opt. Mater. Express* **2019**, *9*, 2067–2075. [CrossRef]
55. Yan, D.X.; Meng, M.; Li, J.S.; Li, X.J. Graphene-assisted narrow bandwidth dual-band tunable terahertz metamaterial absorber. *Front. Phys.* **2020**, *8*, 306. [CrossRef]
56. Kotakoski, J.; Santos-Cottin, D.; Krasheninnikov, A.V. Stability of graphene edges under electron beam: Equilibrium energetics versus dynamic effects. *ACS Nano* **2012**, *6*, 671–676. [CrossRef]
57. Yan, H.; Low, T.; Zhu, W.; Wu, Y.; Freitag, M.; Li, X.; Guinea, F.; Avouris, P.; Xia, F. Damping pathways of mid-infrared plasmons in graphene nanostructures. *Nat. Photon.* **2013**, *7*, 394–399. [CrossRef]
58. Ye, L.; Zeng, F.; Zhang, Y.; Liu, Q.H. Composite graphene-metal microstructures for enhanced multiband absorption covering the entire terahertz range. *Carbon* **2019**, *148*, 317–325. [CrossRef]
59. Qi, L.; Liu, C.; Shah, S.M.A. A broad dual-band switchable graphene-based terahertz metamaterial absorber. *Carbon* **2019**, *153*, 179–188. [CrossRef]
60. Jain, P.; Bansal, S.; Prakash, K.; Sardana, N.; Gupta, N.; Kumar, S.; Singh, A.K. Graphene-based tunable multi-band metamaterial polarization-insensitive absorber for terahertz applications. *J. Mater. Sci. Mater. Electron.* **2020**, *31*, 11878–11886. [CrossRef]
61. Chen, M.; Sun, W.; Cai, J.; Chang, L.; Xiao, X. Frequency-tunable terahertz absorbers based on graphene metasurface. *Opt. Commun.* **2017**, *382*, 144–150. [CrossRef]
62. Wu, D.; Wang, M.; Feng, H.; Xu, Z.X.; Liu, Y.P.; Xia, F.; Zhang, K.; Kong, W.J.; Dong, L.F.; Yun, M.J. Independently tunable perfect absorber based on the plasmonic in double-layer graphene structure. *Carbon* **2019**, *155*, 618–623. [CrossRef]
63. Bao, Z.; Wang, J.; Hu, Z.D.; Chen, Y.; Zhang, C.; Zhang, F. Coordination multi-band absorbers with patterned irrelevant graphene patches based on multi-layer film structures. *J. Phys. D Appl. Phys.* **2021**, *54*, 505306. [CrossRef]
64. Cai, Y.J.; Guo, Y.B.; Zhang, H.Y.; Wang, Y.; Chen, C.Y.; Lin, F.; Zuo, S.K.; Zhou, Y.H. Tunable and polarization-sensitive graphene-based terahertz absorber with eight absorption bands. *J. Phys. D Appl. Phys.* **2021**, *54*, 195106. [CrossRef]
65. Xing, R.; Jian, S. A dual-band THz absorber based on graphene sheet and ribbons. *Opt. Laser Technol.* **2018**, *100*, 129–132. [CrossRef]
66. Zhou, Q.; Zha, S.; Bian, L.A.; Zhang, J.; Ding, L.; Liu, H.; Liu, P. Independently controllable dual-band terahertz metamaterial absorber exploiting graphene. *J. Phys. D Appl. Phys.* **2019**, *52*, 255102. [CrossRef]
67. Ye, L.; Chen, X.; Cai, G.; Zhu, J.; Liu, N.; Liu, Q.H. Electrically tunable broadband terahertz absorption with hybrid-patterned graphene metasurfaces. *Nanomaterials* **2018**, *8*, 562. [CrossRef]
68. Nourbakhsh, M.; Zareian-Jahromi, E.; Basiri, R. Ultra-wideband terahertz metamaterial absorber based on Snowflake Koch Fractal dielectric loaded graphene. *Opt. Express* **2019**, *27*, 32958–32969. [CrossRef]
69. Cai, Y.; Xu, K.D. Tunable broadband terahertz absorber based on multilayer graphene-sandwiched plasmonic structure. *Opt. Express* **2018**, *26*, 31693–31705. [CrossRef]
70. Xu, Z.; Wu, D.; Liu, Y.; Liu, C.; Yu, Z.; Yu, L.; Ye, H. Design of a tunable ultra-broadband terahertz absorber based on multiple layers of graphene ribbons. *Nanoscale Res. Lett.* **2018**, *13*, 143. [CrossRef]
71. Rahmanzadeh, M.; Rajabalipanah, H.; Abdolali, A. Multilayer graphene-based metasurfaces: Robust design method for extremely broadband, wide-angle, and polarization-insensitive terahertz absorbers. *Appl. Opt.* **2018**, *57*, 959–968. [CrossRef] [PubMed]

72. Fardoost, A.; Vanani, F.G.; Amirhosseini, A.; Safian, R. Design of a multilayer graphene-based ultrawideband terahertz absorber. *IEEE Trans. Nanotechnol.* **2016**, *16*, 68–74.
73. Huang, X.; He, W.; Yang, F.; Ran, J.; Gao, B.; Zhang, W.L. Polarization-independent and angle-insensitive broadband absorber with a target-patterned graphene layer in the terahertz regime. *Opt. Express* **2018**, *26*, 25558–25566. [CrossRef] [PubMed]
74. Xiong, H.; Wu, Y.B.; Dong, J.; Tang, M.C.; Jiang, Y.N.; Zeng, X.P. Ultra-thin and broadband tunable metamaterial graphene absorber. *Opt. Express* **2018**, *26*, 1681–1688. [CrossRef] [PubMed]
75. Arik, K.; AbdollahRamezani, S.; Khavasi, A. Polarization insensitive and broadband terahertz absorber using graphene disks. *Plasmonics* **2017**, *12*, 393–398. [CrossRef]
76. Bordbar, A.; Basiry, R.; Yahaghi, A. Design and equivalent circuit model extraction of a broadband graphene metasurface absorber based on a hexagonal spider web structure in the terahertz band. *Appl. Opt.* **2020**, *59*, 2165–2172. [CrossRef]
77. Jiang, Y.; Zhang, H.D.; Wang, J.; Gao, C.N.; Wang, J.; Cao, W.P. Design and performance of a terahertz absorber based on patterned graphene. *Opt. Lett.* **2018**, *43*, 4296–4299. [CrossRef]
78. Han, J.; Chen, R. Tunable broadband terahertz absorber based on a single-layer graphene metasurface. *Opt. Express* **2020**, *28*, 30289–30298. [CrossRef]
79. Chen, F.; Cheng, Y.; Luo, H.A. broadband tunable terahertz metamaterial absorber based on single-layer complementary gammadion-shaped graphene. *Materials* **2020**, *13*, 860. [CrossRef]
80. Ye, L.; Chen, Y.; Cai, G.; Liu, N.; Zhu, J.; Song, Z.; Liu, Q. Broadband absorber with periodically sinusoidally patterned graphene layer in terahertz range. *Opt. Express* **2017**, *25*, 11223–11232. [CrossRef]
81. Ye, L.; Chen, X.; Zhuo, J.; Han, F.; Liu, Q.H. Actively tunable broadband terahertz absorption using periodically square-patterned graphene. *Appl. Phys. Express* **2018**, *11*, 102201. [CrossRef]
82. Biabanifard, M.; Asgari, S.; Biabanifard, S.; Abrishamian, M.S. Analytical design of tunable multi-band terahertz absorber composed of graphene disks. *Optik* **2019**, *182*, 433–442. [CrossRef]
83. Zhong, R.; Yang, L.; Liang, Z.; Wu, Z.; Wang, Y.; Ma, Z.; Fang, Z.; Liu, S.G. Ultrawideband terahertz absorber with a graphene-loaded dielectric hemi-ellipsoid. *Opt. Express* **2020**, *28*, 28773–28781. [CrossRef] [PubMed]
84. Soleymani, A.; Meymand, R.E.; Granpayeh, N. Broadband near-perfect terahertz absorber in single-layered and non-structured graphene loaded with dielectrics. *Appl. Opt.* **2020**, *59*, 2839–2848. [CrossRef]
85. Biabanifard, S.; Biabanifard, M.; Asgari, S.; Asadi, S.; Yagoub, M.C.E. Tunable ultra-wideband terahertz absorber based on graphene disks and ribbons. *Opt. Commun.* **2018**, *427*, 418–425. [CrossRef]
86. Fu, P.; Liu, F.; Ren, G.J.; Su, F.; Li, D.; Yao, J.Q. A broadband metamaterial absorber based on multi-layer graphene in the terahertz region. *Opt. Commun.* **2018**, *417*, 62–66. [CrossRef]
87. Biabanifard, M.; Abrishamian, M.S. Ultra-wideband terahertz graphene absorber using circuit model. *Appl. Phys. A* **2018**, *124*, 826. [CrossRef]
88. Lin, R.; He, X.; Jiang, Z.; Liu, C.; Wang, S.; Kong, Y. Dual-layer graphene based tunable broadband terahertz absorber relying on the coexistence of hybridization and stacking effects. *J. Phys. D Appl. Phys.* **2021**, *54*, 145108. [CrossRef]
89. Liu, W.; Tian, J.P.; Yang, R.C.; Pei, W.H. Design of a type of broadband metamaterial absorber based on metal and graphene. *Curr. Appl. Phys.* **2021**, *31*, 122–131. [CrossRef]
90. Wu, S.; Li, J. Hollow-petal graphene metasurface for broadband tunable THz absorption. *Appl. Opt.* **2019**, *58*, 3023–3028. [CrossRef]
91. Sun, J.Z.; Li, J.S. Broadband adjustable terahertz absorption in series asymmetric oval-shaped graphene pattern. *Front. Phys.* **2020**, *8*, 245. [CrossRef]
92. Yan, D.X.; Li, J.S. Tuning control of broadband terahertz absorption using designed graphene multilayers. *J. Opt.* **2019**, *21*, 075101. [CrossRef]
93. Zhai, Z.; Zhang, L.; Li, X.; Xiao, S. Tunable terahertz broadband absorber based on a composite structure of graphene multilayer and silicon strip array. *Opt. Commun.* **2019**, *431*, 199–202. [CrossRef]
94. Zhu, J.F.; Li, S.F.; Deng, L.; Zhang, C.; Yang, Y.; Zhu, H. Broadband tunable terahertz polarization converter based on a sinusoidally-slotted graphene metamaterial. *Opt. Mater. Express* **2018**, *8*, 1164–1173. [CrossRef]
95. Cheng, Y.; Zhu, X.; Li, J.; Cheney, F.; Luo, H.; Wu, L. Terahertz broadband tunable reflective cross-polarization convertor based on complementary cross-shaped graphene metasurface. *Phys. E Low-Dimens. Syst. Nanostruct.* **2021**, *134*, 114893. [CrossRef]
96. Lin, R.; Lu, F.; He, X.; Jiang, Z.; Liu, C.; Wang, S.; Kong, Y. Multiple interference theoretical model for graphene metamaterial-based tunable broadband terahertz linear polarization converter design and optimization. *Opt. Express* **2021**, *29*, 30357–30370. [CrossRef]
97. Zeng, L.; Huang, T.; Liu, G.B.; Zhang, H.F. A tunable ultra-broadband linear-to-circular polarization converter containing the graphene. *Opt. Commun.* **2019**, *436*, 7–13. [CrossRef]
98. Yao, Z.; Lu, M.; Zhang, C.; Wang, Y. Dynamically tunable and transmissive linear to circular polarizer based on graphene metasurfaces. *J. Opt. Soc. Am. B* **2019**, *36*, 3302–3306. [CrossRef]
99. Fu, Y.; Wang, Y.; Yang, G.; Qiao, Q.; Liu, Y. Tunable reflective dual-band line-to-circular polarization convertor with opposite handedness based on graphene metasurfaces. *Opt. Express* **2021**, *29*, 13373–13387. [CrossRef]
100. Guo, T.; Argyropoulos, C. Broadband polarizers based on graphene metasurfaces. *Opt. Lett.* **2016**, *41*, 5592–5595. [CrossRef]
101. Quader, S.; Zhang, J.; Akram, M.R.; Zhu, W. Graphene-based high-efficiency broadband tunable linear-to-circular polarization converter for terahertz waves. *IEEE J. Sel. Top. Quantum Electron.* **2020**, *26*, 4501008. [CrossRef]

102. Liu, Y.; Qiao, Q.; Fu, Y.; Zhou, X.; Li, R.; Lu, M.; Wang, Y. Reflective triple-band line-to-circular polarization conversion based on diamond-shaped graphene metasurface. *Opt. Mater.* **2021**, *114*, 110984. [CrossRef]
103. Cheng, Y.; Wang, J. Tunable terahertz circular polarization convertor based on graphene metamaterial. *Diam. Relat. Mater.* **2021**, *119*, 108559. [CrossRef]
104. Asgari, S.; Rahmanzadeh, M. Tunable circular conversion dichroism and asymmetric transmission of terahertz graphene metasurface composed of split rings. *Opt. Commun.* **2020**, *456*, 124623. [CrossRef]
105. Amin, M.; Siddiqui, O.; Farhat, M. Linear and circular dichroism in graphene-based reflectors for polarization control. *Phys. Rev. Appl.* **2020**, *13*, 024046. [CrossRef]
106. Zhang, Y.; Feng, Y.; Zhao, J. Graphene-enabled tunable multifunctional metamaterial for dynamical polarization manipulation of broadband terahertz wave. *Carbon* **2020**, *163*, 244–252. [CrossRef]
107. Yao, Z.; Wei, T.; Wang, Y.; Lu, M.; Zhang, C.; Zhang, L. Tunable multifunctional reflection polarizer based on a graphene metasurface. *Appl. Opt.* **2019**, *58*, 3570–3574. [CrossRef]
108. Zhang, H.; Liu, Y.; Liu, Z.; Liu, X.; Liu, G.; Fu, G.; Wang, J.; Shen, Y. Multi-functional polarization conversion manipulation via graphene-based metasurface reflectors. *Opt. Express* **2021**, *29*, 70–81. [CrossRef]
109. Zhang, R.; You, B.; Wang, S.C.; Han, K.; Shen, X.P.; Wang, W. Broadband and switchable terahertz polarization converter based on graphene metasurfaces. *Opt. Express* **2021**, *29*, 24804–24815. [CrossRef]
110. Barkabian, M.; Sharifi, N.; Granpayeh, N. Multi-functional high-efficiency reflective polarization converter based on an ultra-thin graphene metasurface in the THz band. *Opt. Express* **2021**, *29*, 20160–20174. [CrossRef]
111. Zhang, J.; Zhang, K.; Cao, A.; Liu, Y.; Kong, W. Bi-functional switchable broadband terahertz polarization converter based on a hybrid graphene-metal metasurface. *Opt. Express* **2020**, *28*, 26102–26110. [CrossRef] [PubMed]
112. Guan, S.; Cheng, J.; Chen, T.; Chang, S.J. Widely tunable polarization conversion in low-doped graphene-dielectric metasurfaces based on phase compensation. *Opt. Lett.* **2020**, *45*, 1742–1745. [CrossRef] [PubMed]
113. Qiao, Q.; Wang, Y.; Yang, G.; Fu, Y.; Liu, Y. Broadband of linear-to-linear and double-band of linear-to-circular polarization converter based on a graphene sheet with a π-shaped hollow array. *Opt. Mater. Express* **2021**, *11*, 2952–2965. [CrossRef]
114. Guan, S.; Cheng, J.; Chen, T.; Chang, S.J. Bi-functional polarization conversion in hybrid graphene-dielectric metasurfaces. *Opt. Lett.* **2019**, *44*, 5683–5686. [CrossRef] [PubMed]
115. Zhao, J.; Song, J.; Xu, T.; Yang, T.; Zhou, J. Controllable linear asymmetric transmission and perfect polarization conversion in a terahertz hybrid metal-graphene metasurface. *Opt. Express* **2019**, *27*, 9773–9781. [CrossRef]
116. Sajjad, M.; Kong, X.; Liu, S.; Ahmed, A.; Rahman, S.U.; Wang, Q. Graphene-based THz tunable ultra-wideband polarization converter. *Phys. Lett. A* **2020**, *384*, 126567. [CrossRef]
117. Chen, D.; Yang, J.; Huang, J.; Bai, W.; Zhang, J.; Zhang, Z.; Xu, S.; Xie, W. The novel graphene metasurfaces based on split-ring resonators for tunable polarization switching and beam steering at terahertz frequencies. *Carbon* **2019**, *154*, 350–356. [CrossRef]
118. Liu, Z.; Bai, B. Ultra-thin and high-efficiency graphene metasurface for tunable terahertz wave manipulation. *Opt. Express* **2017**, *25*, 8584–8592. [CrossRef]
119. Yahiaoui, R.; Chase, Z.A.; Kyaw, C.; Seabron, E.; Mathews, H.; Searles, T.A. Dynamically tunable single-layer VO_2/metasurface based THz cross-polarization converter. *J. Phys. D Appl. Phys.* **2021**, *54*, 235101. [CrossRef]
120. Zheng, G.G.; Zhou, P.; Chen, Y.Y. Dynamically switchable dual-band mid-infrared absorber with phase-change material $Ge_2Sb_2Te_5$. *Opt. Mater.* **2020**, *99*, 109581. [CrossRef]
121. Mou, N.L.; Liu, X.L.; Wei, T.; Dong, H.X.; He, Q.; Zhou, L.; Zhang, Y.Q.; Zhang, L.; Sun, S.L. Large-scale, low-cost, broadband and tunable perfect optical absorber based on phase-change material. *Nanoscale* **2020**, *12*, 5374–5379. [CrossRef] [PubMed]
122. Dong, G.H.; Qin, C.H.; Lv, T.T.; Sun, M.K.; Lv, B.; Li, Y.X.; Li, P.; Zhu, Z.; Guan, C.Y.; Shi, J.H. Dynamic chiroptical responses in transmissive metamaterial using phase-change material. *J. Phys. D Appl. Phys.* **2020**, *53*, 285104. [CrossRef]
123. Patel, S.K.; Parmar, J. Highly sensitive and tunable refractive index biosensor based on phase change material. *Phys. B* **2021**, *622*, 413357. [CrossRef]
124. Xu, D.D.; Cui, F.P.; Zheng, G.G. Dynamically Switchable Polarization-Independent Triple-Band Perfect Metamaterial Absorber Using a Phase-Change Material in the Mid-Infrared (MIR) Region. *Micromachines* **2021**, *12*, 548. [CrossRef]
125. Gwin, A.H.; Kodama, C.H.; Laurvick, T.V.; Coutu, R.A.; Taday, P.F. Improved terahertz modulation using germanium telluride (GeTe) chalcogenide thin films. *Appl. Phys. Lett.* **2015**, *107*, 031904. [CrossRef]
126. Jeong, H.; Park, J.H.; Moon, Y.H.; Baek, C.W.; Lin, S. Thermal frequency reconfigurable electromagnetic absorber using phase change material. *Sensors* **2018**, *18*, 3506. [CrossRef]
127. Carrillo, S.G.C.; Trimby, L.; Au, Y.Y.; Nagareddy, V.K.; Rodriguez-Hernandez, G.; Hosseini, P.; Rios, C.; Bhaskaran, H.; Wright, C.D. A nonvolatile phase-change metamaterial color display. *Adv. Opt. Mater.* **2019**, *7*, 1801782. [CrossRef]
128. Wang, S.; Kang, L.; Werner, D.H. Active terahertz chiral metamaterials based on phase transition of vanadium dioxide (VO_2). *Sci. Rep.* **2018**, *8*, 189. [CrossRef]
129. Song, Z.; Chen, A.; Zhang, J.; Wang, J. Integrated metamaterial with functionalities of absorption and electromagnetically induced transparency. *Opt. Express* **2019**, *27*, 25196–25204. [CrossRef]
130. Zheng, Z.; Zheng, Y.; Luo, Y.; Yi, Z.; Zhang, J.; Liu, Z.; Yang, W.; Yu, Y.; Wu, X.; Wu, P. Switchable terahertz device combining ultra-wideband absorption and ultra-wideband complete reflection. *Phys. Chem. Chem. Phys.* **2022**, *24*, 2527–2533. [CrossRef]

131. Jeong, Y.G.; Han, S.; Rhie, J.; Kyoung, J.S.; Choi, J.W.; Park, N.; Hong, S.; Kim, B.J.; Kim, H.T.; Kim, D.S. A vanadium dioxide metamaterial disengaged from insulator-to-metal transition. *Nano Lett.* **2015**, *15*, 6318–6323. [CrossRef] [PubMed]
132. Zheng, Z.; Luo, Y.; Yang, H.; Yi, Z.; Zhang, J.; Song, Q.; Yang, W.; Liu, C.; Wu, X.; Wu, P. Thermal tuning of terahertz metamaterial properties based on phase change material vanadium dioxide. *Phys. Chem. Chem. Phys.* **2022**, *24*, 8846–8853. [CrossRef] [PubMed]
133. Butakov, N.A.; Knight, M.W.; Lewi, T.; Iyer, P.P.; Higgs, D.; Chorsi, H.T.; Trastoy, J.; Del Valle Granda, J.; Valmianski, I.; Urban, C.; et al. Broadband electrically tunable dielectric resonators using metal-insulator transitions. *ACS Photonics* **2018**, *5*, 4056–4060. [CrossRef]
134. Tian, X.; Li, Z.Y. An optically-triggered switchable mid-infrared perfect absorber based on phase-change material of vanadium dioxide. *Plasmonics* **2018**, *13*, 1393–1402. [CrossRef]
135. Driscoll, T.; Kim, H.T.; Chae, B.G.; Kim, B.J.; Lee, Y.W.; Jokerst, N.M.; Palit, S.; Smith, D.R.; Di Ventra, M.; Basov, D.N. Memory metamaterials. *Science* **2009**, *325*, 1518–1521. [CrossRef]
136. Hu, F.R.; Li, Y.Y.; Xu, X.L.; Zhou, Y.; Chen, Y.; Zhu, P.D.; Zhao, S.; Jiang, W.Y.; Zhang, W.T.; Han, J.G.; et al. Broadband large-modulation-depth low-current-triggered terahertz intensity modulator based on VO_2 embedded hybrid metamaterials. *Appl. Phys. Express* **2018**, *11*, 092004. [CrossRef]
137. Zhao, S.; Hu, F.R.; Xu, X.L.; Jiang, M.Z.; Zhang, W.T.; Yin, S.; Jiang, W.Y. Electrically triggered dual-band tunable terahertz metamaterial band-pass filter based on Si_3N_4–VO_2–Si_3N_4 sandwich. *Chin. Phys. B* **2019**, *28*, 054203. [CrossRef]
138. Lv, T.; Dong, G.; Qin, C.; Qu, J.; Lv, B.; Li, W.; Zhu, Z.; Li, Y.; Guan, C.; Shi, J. Switchable dual-band to broadband terahertz metamaterial absorber incorporating a VO_2 phase transition. *Opt. Express* **2021**, *29*, 5437–5447. [CrossRef]
139. Yu, P.; Li, Z.W.; Yao, R.; Xu, Y.F.; Cheng, X.H.; Cheng, Z.Q. A tunable dual-band terahertz hybrid metamaterial absorber based on vanadium oxide (VO_2) phase transition. *Eur. Phys. J. D* **2020**, *74*, 5. [CrossRef]
140. Zhao, Y.; Huang, Q.P.; Cai, H.L.; Lin, X.X.; Lu, Y.L. A broadband and switchable VO_2-based perfect absorber at the THz frequency. *Opt. Commun.* **2018**, *426*, 443–449. [CrossRef]
141. Cao, B.Z.; Li, Y.R.; Liu, X.; Fei, H.M.; Zhang, M.D.; Yang, Y.B. Switchable broadband metamaterial absorber/reflector based on vanadium dioxide rings. *Appl. Opt.* **2020**, *59*, 8111–8117. [CrossRef] [PubMed]
142. Wu, G.; Jiao, X.; Wang, Y.; Zhao, Z.; Wang, Y.; Liu, J. Ultra-wideband tunable metamaterial perfect absorber based on vanadium dioxide. *Opt. Express* **2021**, *29*, 2703–2711. [CrossRef] [PubMed]
143. Chen, A.; Song, Z. Tunable Isotropic Absorber with Phase Change Material VO_2. *IEEE Trans. Nanotechnol.* **2020**, *19*, 197–200. [CrossRef]
144. Liu, Y.; Qian, Y.; Hu, F.; Jiang, M.; Zhang, L. A dynamically adjustable broadband terahertz absorber based on a vanadium dioxide hybrid metamaterial. *Results Phys.* **2020**, *19*, 103384. [CrossRef]
145. Ren, Z.; Cheng, L.; Hu, L.; Liu, C.; Jiang, C.; Yang, S.; Ma, Z.; Zhou, C.; Wang, H.; Zhu, X.; et al. Photoinduced Broad-band Tunable Terahertz Absorber Based on a VO_2 Thin Film. *ACS Appl. Mater. Interfaces* **2020**, *12*, 48811–48819. [CrossRef]
146. Chen, X.S.; Li, J.S. Tunable terahertz absorber with multi-defect combination embedded VO_2 thin film structure. *Acta Phys. Sin.* **2020**, *69*, 027801. [CrossRef]
147. Huang, J.; Li, J.N.; Yang, Y.; Li, J.; Li, J.; Zhang, Y.T.; Yao, J.Q. Active controllable dual broadband terahertz absorber based on hybrid metamaterials with vanadium dioxide. *Opt. Express* **2020**, *28*, 7018–7027. [CrossRef]
148. Shabanpour, J.; Beyraghi, S.; Oraizi, H. Reconfigurable honeycomb metamaterial absorber having incident angular stability. *Sci. Rep.* **2020**, *10*, 14920. [CrossRef]
149. Li, J.; Yang, Y.; Li, J.N.; Zhang, Y.T.; Zhang, Z.; Zhao, H.L.; Li, F.Y.; Tang, T.T.; Dai, H.T.; Yao, J.Q. All-optical switchable vanadium dioxide integrated coding metasurfaces for wavefront and polarization manipulation of terahertz beams. *Adv. Theory Simul.* **2020**, *3*, 1900183. [CrossRef]
150. Lv, F.; Wang, L.; Xiao, Z.; Chen, M.; Cui, Z.; Xu, D. Asymmetric transmission polarization conversion of chiral metamaterials with controllable switches based on VO_2. *Opt. Mater.* **2021**, *114*, 110667. [CrossRef]
151. Song, Z.; Chen, A.; Zhang, J. Terahertz switching between broadband absorption and narrowband absorption. *Opt. Express* **2020**, *28*, 2037–2044. [CrossRef] [PubMed]
152. Song, Z.; Zhang, J. Achieving broadband absorption and polarization conversion with a vanadium dioxide metasurface in the same terahertz frequencies. *Opt. Express* **2020**, *28*, 12487–12497. [CrossRef] [PubMed]
153. Yan, D.X.; Meng, M.; Li, J.S.; Li, J.N.; Li, X.J. Vanadium dioxide-assisted broadband absorption and linear-to-circular polarization conversion based on a single metasurface design for the terahertz wave. *Opt. Express* **2020**, *28*, 29843–29854. [CrossRef]
154. Luo, J.; Shi, X.; Luo, X.; Hu, F.; Li, G. Broadband switchable terahertz half-/quarter-wave plate based on metal-VO_2 metamaterials. *Opt. Express* **2020**, *28*, 30861–30870. [CrossRef] [PubMed]
155. Luo, X.; Hu, F.; Li, G. Broadband switchable terahertz half-/quarter-wave plate based on VO_2-metal hybrid metasurface with over/underdamped transition. *J. Phys. D Appl. Phys.* **2021**, *54*, 505111. [CrossRef]
156. Yan, D.X.; Feng, Q.Y.; Yuan, Z.W.; Meng, M.; Li, X.J.; Qiu, G.H.; Li, J.N. Wideband switchable dual-functional terahertz polarization converter based on vanadium dioxide-assisted metasurface. *Chin. Phys. B* **2022**, *31*, 014211. [CrossRef]
157. Chen, L.; Song, Z. Simultaneous realizations of absorber and transparent conducting metal in a single metamaterial. *Opt. Express* **2020**, *28*, 6565–6571. [CrossRef]
158. Schalch, J.S.; Chi, Y.; He, Y.; Tang, Y.; Zhao, X.; Zhang, X.; Wen, Q.Y.; Averitt, R.D. Broadband electrically tunable VO_2-Metamaterial terahertz switch with suppressed reflection. *Microw. Opt. Techn. Let.* **2020**, *62*, 2782–2790. [CrossRef]

159. Liu, C.; Xu, Y.; Liu, H.; Lin, M.; Zha, S. Switchable Metamaterial with Terahertz Buffering and Absorbing Performance. *IEEE Photonics J.* **2021**, *13*, 4600408. [CrossRef]
160. Neupane, M.; Xu, S.Y.; Sankar, R.; Alidoust, N.; Bian, G.; Liu, C.; Belopolski, I.; Chang, T.R.; Jeng, H.T.; Lin, H. Observation of a three-dimensional topological Dirac semimetal phase in high-mobility Cd_3As_2. *Nat. Commun.* **2014**, *5*, 3786. [CrossRef]
161. Wang, Q.; Li, C.Z.; Ge, S.; Li, J.G.; Lu, W.; Lai, J.; Liu, X.; Ma, J.; Yu, D.P.; Liao, Z.M.; et al. Ultrafast broadband photodetectors cased on three-dimensional Dirac semimetal Cd_3As_2. *Nano Lett.* **2017**, *17*, 834–841. [CrossRef] [PubMed]
162. Wang, T.L.; Cao, M.Y.; Zhang, H.Y.; Zhang, Y.P. Tunable terahertz metamaterial absorber based on Dirac semimetal films. *Appl. Opt.* **2018**, *57*, 9555–9561. [CrossRef] [PubMed]
163. Wan, X.; Turner, A.M.; Vishwanath, A.; Savrasov, S.Y. Topological semimetal and Fermi-arc surface states in the electronic structure of pyrochlore iridates. *Phys. Rev. B* **2011**, *83*, 205101. [CrossRef]
164. Fang, C.; Gilbert, M.J.; Dai, X.; Bernevig, B.A. Multi-Weyl topological semimetals stabilized by point group symmetry. *Phys. Rev. Lett.* **2012**, *108*, 266802. [CrossRef]
165. Wu, X.; Zheng, Y.; Luo, Y.; Zhang, J.G.; Yi, Z.; Wu, X.; Cheng, S.; Yang, W.; Yu, Y.; Wu, P. A four-band and polarization-independent BDS-based tunable absorber with high refractive index sensitivity. *Phys. Chem. Chem. Phys.* **2021**, *23*, 26864–26873. [CrossRef]
166. Liang, T.; Gibson, Q.; Ali, M.N.; Liu, M.; Cava, R.J.; Ong, N.P. Ultrahigh mobility and giant magnetoresistance in the Dirac semimetal Cd_3As_2. *Nat. Mater.* **2015**, *14*, 280–284. [CrossRef]
167. Liu, Z.K.; Jiang, J.; Zhou, B.; Wang, Z.J.; Zhang, Y.; Weng, H.M.; Prabhakaran, D.; Mo, S.K.; Peng, H.; Dudin, P.; et al. A stable three-dimensional topological Dirac semimetal Cd_3As_2. *Nat. Mater.* **2014**, *13*, 677–681. [CrossRef]
168. Liu, Z.K.; Zhou, B.; Zhang, Y.; Wang, Z.J.; Weng, H.M.; Prabhakaran, D.; Mo, S.K.; Shen, Z.X.; Fang, Z.; Dai, X.; et al. Discovery of a three-dimensional topological Dirac semimetal Na_3Bi. *Science* **2014**, *343*, 864–867. [CrossRef]
169. Xiong, H.; Ji, Q.; Bashir, T.; Yang, F. Dual-controlled broadband terahertz absorber based on graphene and Dirac semimetal. *Opt. Express* **2020**, *28*, 13884–13894. [CrossRef]
170. Kotov, O.V.; Lozovik, Y.E. Dielectric response and novel electromagnetic modes in three-dimensional Dirac semimetal films. *Phys. Rev. B* **2016**, *93*, 235417. [CrossRef]
171. Wang, Y.; Yi, Y.; Xu, D.; Yi, Z.; Li, Z.; Chen, X.; Jile, H.; Zhang, J.; Zeng, L.; Li, G. Terahertz tunable three band narrowband perfect absorber based on Dirac semimetal. *Phys. E Low-Dimens. Syst. Nanostruct.* **2021**, *131*, 114750. [CrossRef]
172. Liu, G.D.; Zhai, X.; Meng, H.Y. Dirac semimetals based tunable narrowband absorber at terahertz frequencies. *Opt. Express* **2018**, *26*, 11471–11480. [CrossRef] [PubMed]
173. Meng, W.W.; Que, L.C.; Lv, J.; Zhang, L.W.; Zhou, Y.; Jiang, Y.D. A triple-band terahertz metamaterial absorber based on buck Dirac semimetals. *Results Phys.* **2019**, *14*, 102461. [CrossRef]
174. Dai, L.L.; Zhang, Y.P.; Zhang, H.Y.; O'Hara, J.F. Broadband tunable terahertz cross polarization converter based on Dirac semimetals. *Appl. Phys. Express* **2019**, *12*, 075003. [CrossRef]
175. Dai, L.L.; Zhang, Y.P.; Zhang, Y.L.; Liu, S.D.; Zhang, H.Y. Multifunction tunable broadband terahertz device for polarization rotation and linear asymmetric transmission based on Dirac semimetals. *Opt. Commun.* **2020**, *468*, 125802. [CrossRef]
176. Zhang, H.Y.; Yang, C.H.; Liu, M.; Zhang, Y.P. Dual-function tuneable asymmetric transmission and polarization converter in terahertz region. *Results Phys.* **2021**, *25*, 104242. [CrossRef]
177. Wang, T.L.; Zhang, H.Y.; Zhang, Y.; Zhang, Y.P.; Cao, M.Y. Tunable bifunctional terahertz metamaterial device based on Dirac semimetals and vanadium dioxide. *Opt. Express* **2020**, *28*, 17434–17448. [CrossRef]
178. Yang, C.H.; Gao, Q.G.; Dai, L.L.; Zhang, Y.L.; Zhang, H.Y.; Zhang, Y.P. Bifunctional tunable terahertz circular polarization converter based on Dirac semimetals and vanadium dioxide. *Opt. Mater. Express* **2020**, *10*, 2289–2303. [CrossRef]
179. Zhu, H.; Zhang, Y.; Ye, L.; Li, Y.; Xu, Y.; Xu, R. Switchable and tunable terahertz metamaterial absorber with broadband and multi-band absorption. *Opt. Express* **2020**, *28*, 38626–38637. [CrossRef]
180. Liu, Y.; Huang, R.; Ouyang, Z.B. Terahertz absorber with dynamically switchable dual-broadband based on a hybrid metamaterial with vanadium dioxide and graphene. *Opt. Express* **2021**, *29*, 20839–20850. [CrossRef]
181. Liu, W.; Song, Z. Terahertz absorption modulator with largely tunable bandwidth and intensity. *Carbon* **2021**, *174*, 617–662. [CrossRef]
182. Zhang, M.; Song, Z. Terahertz bifunctional absorber based on a graphene-spacer-vanadium dioxide-spacer-metal configuration. *Opt. Express* **2020**, *28*, 11780–11788. [CrossRef] [PubMed]
183. Wang, T.L.; Zhang, Y.P.; Zhang, H.Y.; Cao, M.Y. Dual-controlled switchable broadband terahertz absorber based on a graphene-vanadium dioxide metamaterial. *Opt. Mater. Express* **2020**, *10*, 369–386. [CrossRef]
184. Li, H.; Yu, J. Bifunctional terahertz absorber with a tunable and switchable property between broadband and dual-band. *Opt. Express* **2020**, *28*, 25225–25237. [CrossRef]
185. Wang, Q.Z.; Liu, S.Y.; Ren, G.J.; Zhang, H.W.; Liu, S.C.; Yao, J.Q. Multi-parameter tunable terahertz absorber based on graphene and vanadium dioxide. *Opt. Commun.* **2021**, *494*, 127050. [CrossRef]
186. Li, J.; Zheng, C.L.; Li, J.T.; Zhao, H.L.; Hao, X.R.; Xu, H.; Yue, Z.; Zhang, Y.; Yao, J. Polarization-dependent and tunable absorption of terahertz waves based on anisotropic metasurfaces. *Opt. Express* **2021**, *29*, 3284–3295. [CrossRef]
187. Zhou, Z.; Song, Z. Switchable bifunctional metamaterial for terahertz anomalous reflection and broadband absorption. *Phys. Scr.* **2021**, *96*, 115506. [CrossRef]

188. Liu, H.Y.; Wang, P.P.; Wu, J.L.; Yuan, X.G.; Zhang, Y.; Zhang, X. Switchable and Dual-Tunable Multilayered Terahertz Absorber Based on Patterned Graphene and Vanadium Dioxide. *Micromachines* **2021**, *12*, 619. [CrossRef]
189. Mao, M.; Liang, Y.; Liang, R.; Zhao, L.; Xu, N.; Guo, J.; Wang, F.; Meng, H.; Liu, H.; Wei, Z. Dynamically temperature-voltage controlled multifunctional device based on VO_2 and graphene hybrid metamaterials: Perfect absorber and highly efficient polarization converter. *Nanomaterials* **2019**, *9*, 1101. [CrossRef]
190. Wang, S.Z.; Xu, R.H.; Qin, Z.J.; Liu, H.Q.; Deng, S.J.; Chen, M.; Cheng, Y.; Yuan, L.B. Wide-range tunable, dual-band, background refractive index insensitive terahertz absorber based on graphene and Dirac semimetal. *Opt. Eng.* **2021**, *60*, 027102. [CrossRef]
191. Li, Y.; Zhai, X.; Xia, S.X.; Li, H.J.; Wang, L.L. Active control of narrowband total absorption based on terahertz hybrid Dirac semimetal-graphene metamaterials. *J. Phys. D Appl. Phys.* **2020**, *53*, 205106. [CrossRef]
192. Liang, Y.; Koshelev, K.; Zhang, F.; Lin, H.; Lin, S.; Wu, J.; Jia, B.; Kivshar, Y. Bound states in the continuum in anisotropic plasmonic metasurfaces. *Nano Lett.* **2020**, *20*, 6351–6356. [CrossRef] [PubMed]
193. Tang, B.; Yang, N.; Song, X.; Song, X.; Jin, G.; Su, J. Triple-Band Anisotropic Perfect Absorbers Based on α-Phase MoO_3 Metamaterials in Visible Frequencies. *Nanomaterials* **2021**, *11*, 2061. [CrossRef]
194. Dereshgi, A.S.; Folland, T.G.; Murthy, A.A.; Song, X.L.; Tanriover, I.; Dravid, V.D.; Caldwell, J.D.; Aydin, K. Lithography-free IR polarization converters via orthogonal in-plane phonons in α-MoO_3 flakes. *Nat. Commun.* **2020**, *11*, 5771. [CrossRef] [PubMed]
195. Zhou, F.; Qin, F.; Yi, Z.; Yao, W.T.; Liu, Z.; Wu, X.; Wu, P. Ultra-wideband and wide-angle perfect solar energy absorber based on Ti nanorings surface plasmon resonance. *Phys. Chem. Chem. Phys.* **2021**, *23*, 17041–17048. [CrossRef]
196. Zhao, F.; Lin, J.C.; Lei, Z.; Yi, Z.; Qin, F.; Zhang, J.; Liu, L.; Wu, X.; Yang, W.; Wu, P. Realization of 18.97% theoretical efficiency of 0.9 μm Thick c-Si/ZnO Heterojunction Ultrathin-film Solar Cells via Surface Plasmon Resonance Enhancement. *Phys. Chem. Chem. Phys.* **2022**, *24*, 4871–4880. [CrossRef]
197. Yu, P.; Besteiro, L.V.; Huang, Y.J.; Wu, J.; Fu, L.; Tan, H.H.; Jagadish, C.; Wiederrecht, G.P.; Govorov, A.O.; Wang, Z.M. Broadband metamaterial absorbers. *Adv. Opt. Mater.* **2019**, *7*, 1800995. [CrossRef]